Anderson localization of a weakly interacting one-dimensional Bose gas

T. Paul,[1,2] M. Albert,[1] P. Schlagheck,[3,4] P. Leboeuf,[1] and N. Pavloff[1]
[1]*Laboratoire de Physique Théorique et Modèles Statistiques, CNRS, Université Paris Sud, UMR 8626, 91405 Orsay Cedex, France*
[2]*Institut für Theoretische Physik, Universität Heidelberg, Philosophenweg 19, 69120 Heidelberg, Germany*
[3]*Institut für Theoretische Physik, Universität Regensburg, 93040 Regensburg, Germany*
[4]*Mathematical Physics, Lund Institute of Technology, P.O. Box 118, 22100 Lund, Sweden*
(Received 1 July 2009; published 17 September 2009; publisher error corrected 21 September 2009)

We consider the phase coherent transport of a quasi-one-dimensional beam of Bose-Einstein condensed particles through a disordered potential of length L. Among the possible different types of flow we identified [T. Paul, P. Schlagheck, P. Leboeuf, and N. Pavloff, Phys. Rev. Lett. **98**, 210602 (2007)], we focus here on the supersonic stationary regime where Anderson localization exists. We generalize the diffusion formalism of Dorokhov-Mello-Pereyra-Kumar to include interaction effects. It is shown that interactions modify the localization length and also introduce a length scale L^* for the disordered region, above which most of the realizations of the random potential lead to time-dependent flows. A Fokker-Planck equation for the probability density of the transmission coefficient that takes this effect into account is introduced and solved. The theoretical predictions are verified numerically for different types of disordered potentials. Experimental scenarios for observing our predictions are discussed.

DOI: 10.1103/PhysRevA.80.033615 PACS number(s): 03.75.−b, 05.60.Gg, 42.65.Tg, 72.15.Rn

I. INTRODUCTION

The absence of diffusion of waves in disordered media was predicted by Anderson 50 years ago [1]. Originally proposed in the context of electronic transport in disordered crystals, it has since been observed for different types of waves, including light and sound. Recently, direct observations of the Anderson localization by disorder [2] and of a localization transition by quasiperiodic potentials [3] of quasi-one-dimensional (1D) matter waves of ultracold atoms were reported. These experiments pave the way to the observation of new phenomena and shed new light on long standing problems, among which the question of possible Anderson localization in presence of interactions.

In the present paper we consider the case of an atomic vapor described as a weakly interacting Bose gas in the presence of a weak disorder (what is meant by "weak" here will be made quantitative in Sec. II). In this configuration it has been shown theoretically in Refs. [4,5] and supported by numerical simulations in Ref. [6] that a small amount of disorder does not drastically alter the *equilibrium* properties of the system, but merely decreases the condensate and superfluid fractions. Furthermore, even in the 1D limit considered in the present work, it has been experimentally demonstrated in Refs. [7,8] that one can observe global phase coherence in the presence of disorder and remain far from, say, the Bose glass phase originally proposed by Giamarchi and Schulz and Fisher *et al.* [9,10].

Here, we are interested in *transport* properties. Specifically, we study a quasi-1D weakly interacting Bose-Einstein condensate (BEC), propagating through a disordered potential. In this context, localization has been theoretically studied mainly for effective *attractive* interactions (see, e.g., [11] and references therein), with less attention on the *repulsive* case we consider here (see, however, Refs. [12,13]). In the absence of an external potential, (repulsive) interactions make the system superfluid and introduce a new characteristic speed in the system, the speed of sound c. As mentioned above, when the speed V of the BEC relative to the external potential tends to zero, the addition of a weak random potential preserves superfluidity, although with a reduced superfluid fraction. What happens as V increases? This question was investigated in a previous publication [14], where the disordered potential, of length L, was modeled by a series of randomly located delta peaks. For small velocities $V/c \ll 1$, perturbation theory shows that the superfluidity is preserved, e.g., the flow is dissipationless and with a perfect transmission. In contrast, in the high speed limit $V/c \gg 1$, where the kinetic energy dominates over the interaction energy, the transport properties of the BEC are deeply altered and tend to those of the noninteracting gas, displaying an exponential damping of the transmission with length L, a behavior characteristic of the strong Anderson localization. Thus, two limiting cases of stationary flow have been identified [14], with contrasting transport properties: superfluidity in the deep subsonic regime and Anderson localization in the deep supersonic one. In between, in the region $V \sim c$ where both interaction and kinetic energies are important, it was shown that stationary scattering solutions do not exist: one reaches a regime of time-dependent flows with more or less (depending on the speed) complex density excitations. The range of speeds around c where this phenomenon is observed increases as the length L increases. The different types of existing flows are summarized in Fig. 1.

In the present study we concentrate on the supersonic stationary region of the phase diagram [gray (light blue online), $V/c > 1$ region in Fig. 1]. In this domain we provide analytical and numerical evidence of Anderson localization in the presence of interaction for different types of disorder. We compute analytically the interaction-dependent localization length as well as the corresponding distribution of transmission coefficients. We also explain the disappearance of the supersonic stationary flow observed at a given velocity for increasing length of the disordered sample. This onset of time dependence is an important qualitative effect revealed

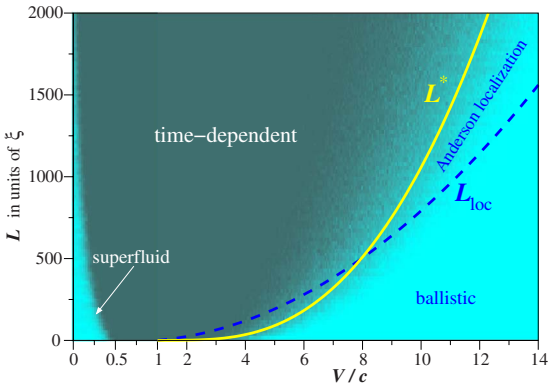

FIG. 1. (Color online) Transport of a quasi-1D BEC with velocity V through a disordered potential U_δ consisting in a series of uncorrelated delta peaks extending over a domain of size L [cf. Eq. (21) and the discussion in Sec. V C]. Dark region: time-dependent flow; light gray (light blue online) regions: stationary flow. In the supersonic case, the yellow solid line corresponds to the threshold L^* between these two domains as determined from Eq. (81). The blue dashed line is the localization length $L_{\rm loc}$ (87). The supersonic region below $L_{\rm loc}$ denoted as "ballistic" corresponds to the region where the perturbation theory of Sec. V A applies. Note the enlarged scale for $V/c \in [0,1]$.

by our study. We show that it is directly connected to interaction effects and provide an analytical estimate of the length L^* of the disordered region above which most of the realizations of the random potential lead to time-dependent flows (see Fig. 1).

The paper is organized as follows. In Sec. II we present the model and identify its range of validity. In Sec. III we take some time to properly define the transmission coefficient of a Bose-condensed beam over an obstacle. In Sec. IV we introduce the different types of disordered potentials studied in the present work. In Sec. V we present analytical and numerical results showing that Anderson localization is indeed possible in the supersonic regime. We consider the three possible supersonic regimes: perturbative (Sec. V A), Anderson localized (Sec. V B), and onset of time dependence (Sec. V C). In Sec. VI we discuss experimental strategies and possible signatures for the observation of Anderson localization in an interacting Bose-Einstein condensate. Finally, we present our conclusions in Sec. VII. Some technical points are given in appendixes. In Appendix A we derive the probability distribution of transmission in a special case (perturbative regime and correlated Gaussian potential). In Appendix B we present the derivation of the Fokker-Plank equation (66) for the distribution of the transmission coefficients.

II. MODEL

We study here the transport properties of a quasi-1D Bose-Einstein condensate formed of particles of mass m, experiencing a repulsive effective interaction [characterized by the three-dimensional (3D) s-wave scattering length $a>0$], in the presence of an obstacle represented by the external potential U. The potential is not necessarily disordered at this point; the only restriction we impose throughout the present work is that it should have a finite extent, i.e., $U(x)\to 0$ when $x\to\pm\infty$. The configuration we consider corresponds to the "1D mean-field regime" [15] (see also the discussion in Ref. [16]), where the system is described by a 1D order parameter $\psi(x,t)$ depending on a single spatial variable: the coordinate x along the direction of propagation. $\psi(x,t)$ obeys the nonlinear Schrödinger equation

$$i\hbar\frac{\partial\psi}{\partial t} = -\frac{\hbar^2}{2m}\frac{\partial^2\psi}{\partial x^2} + [U(x-Vt) + g|\psi|^2 - \mu]\psi. \qquad (1)$$

In all the present work we choose to work in the "laboratory frame" where the condensate is initially at rest. Equation (1) describes its 1D dynamics in the presence of an obstacle moving at constant velocity V in this frame, which corresponds to the experimental situation where an obstacle is swept through a condensate initially at rest (see, e.g., Refs. [17–19]). On the theoretical side, one should imagine that, from an initial static configuration where the condensate is at rest with $U\equiv 0$, the potential intensity and the speed have been slowly ramped up to a point where the condensate dynamics is described by Eq. (1). We choose $V>0$; this corresponds to a potential moving from left to right in the laboratory frame.

The reduction of the motion of the condensate to a single spatial dimension is typically achieved through a transverse harmonic confining potential of pulsation $\omega_\perp$. We choose a normalization such that $n(x,t)=|\psi(x,t)|^2$ is the linear density of the condensate. In this case, the interaction among particles results in Eq. (1) in the nonlinear term $g|\psi|^2$, with $g=2\hbar\omega_\perp a$ [20–22].

In the stationary regime, where the flow is time-independent in the frame moving with the potential, ψ depends on x and t only through the variable $X=x-Vt$. The appropriate boundary condition is $\psi(X\to-\infty)=\sqrt{n_0}$ (where n_0 is a constant) (see [22] and the discussion in Sec. III A below). The condensate is then characterized by a chemical potential $\mu=gn_0$, a speed of sound $c=(gn_0/m)^{1/2}$, and a healing length $\xi=\hbar/(mc)$.

It is customary to characterize the transverse confinement via the "harmonic-oscillator length" $a_\perp=(\hbar/m\omega_\perp)^{1/2}$. With n_1 denoting a typical order of magnitude of $n(x,t)$, the 1D mean-field regime in which Eq. (1) is valid corresponds to a density range such that

$$(a/a_\perp)^2 \ll n_1 a \ll 1. \qquad (2)$$

In this domain the wave function of the condensate can be factorized in a transverse part and in a longitudinal part [20–22]. The transverse wave function is Gaussian (this is ensured by the condition $n_1 a\ll 1$); the longitudinal one is of the form $\psi(x,t)\exp\{-i\mu t/\hbar\}$ and $\psi(x,t)$ satisfies Eq. (1) [21,22]. The left-hand side (l.h.s.) inequality in Eq. (2) prevents the system to enter in the Tonks-Girardeau regime. More precisely, a general analysis of 1D Bose gas shows that at zero temperature no BEC is possible [23]. This results in a algebraic decrease of the one-body density matrix monitored by phase fluctuations occurring over a phase-coherence length $L_\phi=\xi\exp\{\pi a_\perp(n_1/2a)^{1/2}\}$ [24,25]. Hence, the results

obtained using Eq. (1) are valid if they describe structures with a characteristic length scale smaller than L_ϕ. The l.h.s. inequality in Eq. (2) ensures that L_ϕ is exponentially large compared to the healing length. If one considers, for instance, ^{87}Rb or ^{23}Na atoms in a guide with a transverse confinement characterized by $\omega_\perp = 2\pi \times 500$ Hz, the ratio $a/a_\perp$ is roughly of order 10^{-2} and restriction (2) still allows the density to vary over four orders of magnitude.

Even if the mean-field approach is legitimate in one dimension, the effects of disorder have to be taken into account with some care. It may well be that the introduction of a disordered potential U in Eq. (1) modifies the properties of the ground state. This is indeed the case as shown in Refs. [4,5]: a disordered potential decreases the condensate and the superfluid fraction, but the effects are weak provided the intensity of the disorder remains weak (see Ref. [26] for an extension to finite temperature). More precisely, in the case of a disorder formed by randomly spaced delta impurities with density n_δ (see Sec. IV A) one can show [14,27] that, in the dilute impurity limit, at $V=0$ the nonsuperfluid fraction (normal part) is proportional to $n_\delta \xi (\xi/b)^2$ [the notations are those of Eq. (21)] and thus remains small provided the dimensionless coefficient (ξ/b) is small (weak disorder limit). At finite V, the normal fraction is multiplied by a factor $[1-(V/c)^2]^{-3/2}$ (see Ref. [14]), which diverges when $V=c$. One thus expects the mean-field approach to fail near the region $V \simeq c$ of Fig. 1. This is supported by the numerical results presented in [28]. Hence, in the center of the time-dependent region of Fig. 1, we cannot trust the results obtained from Eq. (1). However, far from this region, the 1D mean-field approach is expected to be valid even in presence of (weak) disorder, as experimentally demonstrated in Refs. [7,8].

III. DEFINITION OF THE TRANSMISSION

In the present work we characterize the localization properties of the condensate in the random potential by studying the transmission coefficient. Equation (1) being nonlinear, the definition of transmission and reflection coefficients needs to be treated with special care. This is the purpose of the present section where we first define the stationary regime (Sec. III A) and then the transmission coefficient within this regime (Sec. III B).

A. Stationary regime

It is customary to perform a Madelung transformation and to write $\psi(x,t) = \sqrt{n(x,t)}\exp\{iS(x,t)\}$, where $n(x,t)$ is the density and $\hbar \partial_x S/m = v(x,t)$ is the local velocity. From Eq. (1) one can check that they verify the continuity equation

$$\partial_t n + \partial_x (nv) = 0. \tag{3}$$

The stationary regime is defined as the regime where the system is at rest in the frame moving with the obstacle. In this case, in the laboratory frame, ψ, S, n, and v are time dependent, but they depend on x and t only through the variable $X = x - Vt$. It is then possible to get a first integral of Eq. (3) under the form

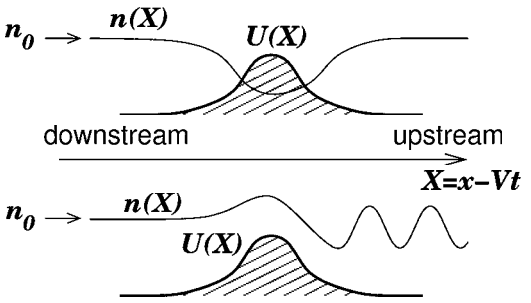

FIG. 2. Schematic representation of the typical density profiles. The upper plot corresponds to a subsonic stationary profile, while the lower one corresponds to a supersonic stationary profile. The potential moves from left to right, and the upstream (downstream) region thus corresponds to the region $X \to +\infty$ $(X \to -\infty)$. In both plots the potential is represented by a thick solid line (hatched down to zero) and the density profile is represented by a thin solid line.

$$n(X)\left(\frac{\hbar}{m}\frac{dS}{dX} - V\right) = C^{st}. \tag{4}$$

In the case of subsonic $(V<c)$ and stationary motion, the flow is superfluid and the order parameter is only affected in the vicinity of the obstacle, with $n(X \to \pm\infty) = n_0$ and $v(X \to \pm\infty) = 0$ [22,29].

For $V>c$, a regime of stationary flow also exists but in this case the obstacle induces density oscillations with a pattern stationary in its rest frame [22]. This means that in the laboratory frame the phase velocity of these waves is identical to the velocity V of the obstacle. On the other hand, the energy transferred from the obstacle to the fluid propagates with the group velocity, which in the case of Bogoliubov excitations is greater than the phase velocity—i.e., as just argued—than V. As a consequence, radiation conditions require that the wake is always located ahead of the obstacle, i.e., upstream, with no long-range perturbation of the fluid on the downstream side [22,30]. This means that in this case the flow far in the downstream region remains unperturbed, with $n(X \to -\infty) = n_0$ and $v(X \to -\infty) = 0$. The two possible stationary configurations (subsonic and supersonic) are represented in Fig. 2. Hence, in any stationary configuration (subsonic or supersonic), the above reasoning fixes the integration constant in the right-hand side (r.h.s.) of Eq. (4) to its value at $X \to -\infty$, i.e., $-n_0 V$.

In the stationary regime one gets from Eqs. (1) and (4)

$$U(X)\frac{dA^2}{dX} = \frac{d}{dX}\left\{\frac{\hbar^2}{2m}\left(\frac{dA}{dX}\right)^2 + W(A)\right\}, \tag{5}$$

where $A(X) = \sqrt{n(X)/n_0}$ and

$$W(A) = \frac{m}{2}(A^2-1)\left[c^2 + V^2 - c^2A^2 - \frac{V^2}{A^2}\right]. \tag{6}$$

B. Transmission coefficient

In this section we restrict the analysis to the stationary regime of Sec. III A and define the transmission of the condensate through the obstacle represented by a potential U

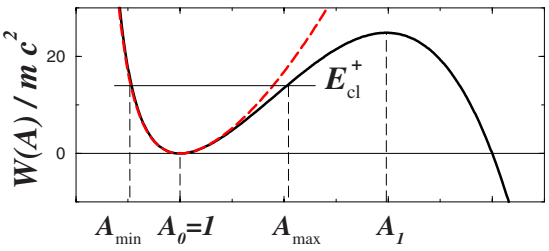

FIG. 3. (Color online) W as a function of $A=|\psi|/\sqrt{n_0}$ (drawn for $V/c=4$). The fictitious particle has a classical energy $E_{\rm cl}^{+}$ when $X\to+\infty$. The (red) dashed line corresponds to an approximation of $W(A)$ by $\hbar^2\kappa^2(A-1/A)^2/(2m)$, obtained by keeping only the first term in expansion (13).

(not necessarily disordered) verifying $U(|x|\to\infty)=0$. As the wave equation (1) is nonlinear, one cannot, in general, properly define reflection and transmission coefficients since it is generally not possible to disentangle incoming and reflected waves in the nonlinear flow upstream the obstacle. However, following a procedure devised in Ref. [31] (see also [32]), we will show that one can define a transmission and a reflection coefficient in the limit of small nonlinearity as well as in the limit of weak reflection and arbitrary nonlinearity.

Outside the scattering region, $U(X)=0$ and one can get a first integral of Eq. (5) under the form

$$\frac{\hbar^2}{2m}\left(\frac{dA}{dX}\right)^2+W(A)=E_{\rm cl}^{\pm}\quad\text{when}\quad X\to\pm\infty, \tag{7}$$

which defines the "free" asymptotic density profiles. $E_{\rm cl}^{\pm}$ in Eq. (7) are integration constants. The boundary condition discussed in the previous section imposes $A=1$ and $dA/dX=0$ when $X\to-\infty$. This fixes the value $E_{\rm cl}^{-}=0$. The value of $E_{\rm cl}^{+}$ at $+\infty$ has to be determined by the integration of Eq. (1) (cf. Ref. [22]). Equation (7) expresses the energy conservation for a fictitious classical particle with "mass" $\hbar^2/m$, "position" A, and "time" X, evolving in a potential W (whose typical shape is displayed in Fig. 3). This type of analysis is common in the study of nonlinear equations such as Eq. (1); see, e.g., the review [33] (the first time we found its use is in Ref. [34]). It is employed here as a convenient tool for getting intuition about the behavior of the solution of the Gross-Pitaevskii equation (see below).

From now on we restrict to the supersonic stationary regime where an imperfect transmission occurs (in the subsonic stationary regime one has perfect transmission). In this case the fictitious particle is initially (i.e., when $X\to-\infty$) at rest at the bottom of the potential W with $E_{\rm cl}^{-}=0$. The behavior of A for $X\to+\infty$ depends on the value of $E_{\rm cl}^{+}$. A stationary solution exists only if $A(X\to+\infty)$ remains bounded, i.e., if $E_{\rm cl}^{+}<W(A_1)$ (where A_1 corresponds to the local maximum of W; see Fig. 3). In this case, the asymptotic behavior of $A(X)$ corresponds to oscillations between the values $A_{\rm min}$ and $A_{\rm max}$ defined in Fig. 3.

For future references we note that $W(A)$ is zero when $A=A_0=1$ and when $A=V/c$, and that the derivative dW/dA is zero when $A=A_0=1$ and when $A=A_1$, with

$$A_1=\frac{V}{2c}\left(1+\sqrt{1+\frac{8c^2}{V^2}}\right)^{1/2}. \tag{8}$$

At large velocity, when $V\gg c$, one has

$$A_1=\frac{V}{\sqrt{2}c}+O\left(\frac{1}{V/c}\right), \tag{9}$$

$$W(A_1)=\frac{mV^4}{8c^2}+O\left(\frac{V^2}{c^2}\right). \tag{10}$$

Writing $A^2(X)=\rho(X)=1+\delta\rho(X)$ we now argue that, following Ref. [31], one can write a perturbative version of Eq. (7) in a limit where

$$|\delta\rho(X)|\ll\left|\frac{V^2}{c^2}-1\right|. \tag{11}$$

We emphasize that restriction (11) corresponds to $|\delta\rho|\ll1$ (i.e., small oscillations) only when V is of order of c or smaller. The approach developed below is however able to tackle large relative density oscillations ($|\delta\rho|\gg1$) at large velocities ($V\gg c$) [35]. In this sense it will allow us to penetrate in the nonperturbative regime where the upstream density oscillations are large and the transmission is low.

Using the variable ρ, we write Eq. (7) in the upstream region ($X\to+\infty$) as

$$\frac{\hbar^2}{2m}\left(\frac{d\rho}{dX}\right)^2+8F(\rho)=8\rho E_{\rm cl}^{+}, \tag{12}$$

where $F(\rho)=\rho W(A=\sqrt{\rho})$. A simple limited expansion around $\rho=1$ yields

$$F(\rho)\simeq\frac{\hbar^2\kappa^2}{2m}(\delta\rho)^2+\frac{mc^2}{2}(\delta\rho)^3+\cdots, \tag{13}$$

where $\delta\rho(X)=\rho(X)-1$ and

$$\kappa=\frac{m}{\hbar}|V^2-c^2|^{1/2},\quad\left|\frac{V^2}{c^2}-1\right|=\kappa^2\xi^2. \tag{14}$$

The second term in the r.h.s. of expansion (13) is small compared to the first one precisely in the limit (11). In the following we restrict to this regime and neglect the second term of the r.h.s. of Eq. (13). This corresponds to approximating the exact $W(A)$ by the (red online) dashed line in Fig. 3 and to write Eq. (12) under the form

$$\left(\frac{d\delta\rho}{dX}\right)^2+4\kappa^2(\delta\rho)^2=16\kappa^2\lambda(1+\delta\rho), \tag{15}$$

where the dimensionless parameter λ is defined by

$$\lambda=\frac{mE_{\rm cl}^{+}}{2\hbar^2\kappa^2}. \tag{16}$$

The solution of Eq. (15) is

$$\frac{n(X)}{n_0}=\rho(X)=1+2\lambda+2\Lambda\cos(2\kappa X+\theta), \tag{17}$$

where

$$\Lambda = \sqrt{\lambda^2 + \lambda} \tag{18}$$

and θ is a phase factor. We recall that Eq. (17) describes the density oscillations in the upstream region $X \to +\infty$. These oscillations can be described as the sum of incident and reflected waves ($\psi_{\rm inc}$ and $\psi_{\rm ref}$) of the form

$$\psi_{\rm inc}(X) = \sqrt{n_0(1+\lambda)}\, \exp(-i\kappa X),$$

$$\psi_{\rm ref}(X) = \sqrt{n_0\lambda}\, \exp(i\kappa X + i\theta). \tag{19}$$

This analysis allows one to determine the reflection and the transmission coefficients as

$$R = \frac{|\psi_{\rm ref}|^2}{|\psi_{\rm inc}|^2} = \frac{\lambda}{1+\lambda}, \quad T = 1 - R = \frac{1}{1+\lambda}. \tag{20}$$

Of course the sum of the incident $\psi_{\rm inc}$ and the reflected $\psi_{\rm ref}$ waves (19) is an approximate solution of the nonlinear Schrödinger equation (1), which is only valid in regime (11), i.e., in the regime of arbitrary interaction and small transmission ($\lambda \ll 1$), or in the regime of arbitrary transmission and small interaction ($V \gg c$).

IV. DIFFERENT TYPES OF DISORDER

Up to this point we presented a theory valid for any potential of finite extent. From now on we concentrate on the particular case of random potentials. We denote $U(x)$ an arbitrary random potential and use a subscript when dealing with one of the particular cases defined below.

A. Potential formed by a series of δ peaks

The first potential of interest, analyzed in Ref. [14], is a series of N randomly located identical delta peaks of the form

$$U_\delta(x) = \frac{\hbar^2}{mb} \sum_{i=1}^{N} \delta(x - x_i). \tag{21}$$

The intensity of the peaks is measured by the (nonrandom) positive quantity b. The scatterers have random uncorrelated positions $0 = x_1 \le x_2 \le x_3 \cdots$, with mean density n_δ and average separation $l_\delta = 1/n_\delta$. Hence, the potential extends over a mean length $L = (N-1) l_\delta$.

Denoting henceforth the disorder average by $\langle \cdots \rangle$ for x and x' inside the disordered region, one gets the mean value

$$\langle U_\delta(x) \rangle = \frac{\hbar^2 n_\delta}{mb} \tag{22}$$

and the irreducible two-point correlation function

$$\langle U_\delta(x) U_\delta(x') \rangle - \langle U_\delta \rangle^2 = \sigma(\hbar^2/m)^2 \delta(x - x'), \tag{23}$$

where

$$\sigma = \frac{n_\delta}{b^2}. \tag{24}$$

B. Correlated Gaussian potential

Another commonly used model of disorder is provided by Gaussian random processes with zero average. We consider here potentials which are nonzero only over a region of finite extent (with typical size L) and generate them in the following way (see, e.g., Chap. 5 of Ref. [36] and references therein): let us consider a Gaussian white noise $\eta(x)$ extending over all the real axis, with zero mean and second moment $\langle \eta(x)\eta(y) \rangle = \delta(x-y)$. Then for a given function $w(x)$ one defines

$$U_g(x) = \frac{\hbar^2 \sqrt{\sigma}}{m} \int_0^L w(x-y)\, \eta(y) dy, \tag{25}$$

where σ is a parameter characterizing the disorder and whose meaning is explained below. If w were a delta function, then U_g would be a Gaussian white noise over $[0, L]$ (and zero everywhere else). The actual function $w(x)$ has a finite extension, and this induces finite correlations in the disordered potential.

From Eq. (25) it is clear that $\langle U_g \rangle = 0$. If the domain of integration in the r.h.s. of Eq. (25) were extended to all $\mathbb{R}$, U_g would have a Gaussian distribution

$$\mathcal{P}(U_g) = \frac{\exp\left[-\dfrac{U_g^2}{2\Sigma^2} \right]}{\sqrt{2\pi\Sigma^2}}, \tag{26}$$

where

$$\Sigma^2 = \sigma(\hbar^2/m)^2 \int_{\mathbb{R}} w^2(x) dx. \tag{27}$$

Defining the correlation function C as

$$\langle U_g(x) U_g(x') \rangle - \langle U_g \rangle^2 = \sigma(\hbar^2/m)^2 C(x - x'), \tag{28}$$

one would get in this case

$$C(x) = \int_{\mathbb{R}} dy\; w(x+y) w(y), \tag{29}$$

with a Fourier transform

$$\hat{C}(q) = \int_{\mathbb{R}} dx\; C(x) e^{-iqx} = |\hat{w}(q)|^2, \tag{30}$$

where $\hat{w}$ is the Fourier transform of w.

Imposing here the normalization condition

$$\int_{\mathbb{R}} w(x) dx = 1, \tag{31}$$

leads to a two-point correlation function (28), which is—as in Eq. (23)—of the form of $\sigma(\hbar^2/m)^2$ multiplied by a function whose integral over x equals unity [$C(x)$ in Eq. (28) instead of $\delta(x)$ in Eq. (23)]. Thus, with definition (25) and normalization (31), σ plays for disorder (25) the same role as n_δ/b^2 [Eq. (24)] for disorder (21): it characterizes the amplitude of the fluctuations of the potential. The typical extent of $w(x)$ will in turn characterize the range of the correlations.

Since U_g as given by Eq. (25) is typically nonzero only over a region of finite extent, Eqs. (28) and (29) are only correct if x and x' are inside this region. More precisely, they should be in this region, at a distance from 0 or L larger than

the typical extent ℓ_c of the function w. In the following we always consider the case where L is very large compared to ℓ_c (otherwise, one could simply not speak of a disordered region) and it is clear that the characteristics of the disorder are properly defined only inside the disordered region.

We consider two special cases of correlation corresponding to different forms of w: a Lorentzian

$$w_L(x) = \frac{1}{\pi}\frac{\ell_c/2}{(\ell_c/2)^2 + x^2} \tag{32}$$

and a Gaussian

$$w_G(x) = \frac{1}{\ell_c\sqrt{\pi}}\exp\left(-\frac{x^2}{\ell_c^2}\right). \tag{33}$$

We denote the corresponding potentials by U_L and U_G. For the correlation functions one gets, respectively,

$$C_L(x) = \frac{\ell_c/\pi}{\ell_c^2 + x^2}, \quad \hat{C}_L(q) = e^{-\ell_c|q|}, \tag{34}$$

$$C_G(x) = \frac{e^{-x^2/(2\ell_c^2)}}{\sqrt{2\pi\ell_c^2}}, \quad \hat{C}_G(q) = e^{-q^2\ell_c^2/2}. \tag{35}$$

In both cases ℓ_c is the typical correlation radius.

The choice of a Lorentzian correlated disordered potential originates from experimental and theoretical results in the case of microfabricated guides. In this type of setting, the atoms are magnetically guided over a chip [37]. Unavoidable imperfections and irregularities in the design of the circuit induce fluctuations in the current which, in turn, result in a random contribution to the magnetic field used for guiding the atoms. Thus, the potential seen by the atoms has a random component which is typically Lorentzian correlated, with a correlation length ℓ_c which decreases when the distance between the guide and the chip increases [13,38–40]. The Gaussian correlated potential U_G is more academic, but by comparison with the results obtained with U_L it allows one to check what is really specific to the Lorentzian case and what is a mere effect of finite correlation length.

C. Speckle potential

Another experimentally relevant type of disorder is the so-called speckle potential, which is generated by an optical speckle field produced by a laser beam passing through a diffusing plate [41–43]. The corresponding potential will be denoted by U_S and may be mathematically generated as follows [44]:

$$U_S(x) = \frac{\hbar^2\sqrt{\sigma}}{m}\left|\int_0^L w_S(x-y)[\eta_1(y) + i\eta_2(y)]dy\right|^2, \tag{36}$$

where η_1 and η_2 are two independent Gaussian white noise processes of zero mean with $\langle \eta_\alpha(x)\eta_{\alpha'}(x')\rangle = \delta(x-x')\delta_{\alpha\alpha'}$ (α and $\alpha' = 1$ or 2).

Here also, we characterize the disorder by studying its statistical properties in the limit where the domain of integration in the r.h.s. of Eq. (36) is extended to all $\mathbb{R}$. In this case one gets

$$\mathcal{P}(U_S) = \frac{\exp\left(-\frac{U_S}{2\Sigma^2}\right)}{2\Sigma^2}, \tag{37}$$

where Σ is given by formula (27) (replacing w by w_S). This yields $\langle U_S\rangle = 2\Sigma^2$ and the correlation function defined in Eq. (28) reads here

$$C_S(x-x') = \frac{1}{\sigma(\hbar^2/m)^2}[\langle U_S(x)U_S(x')\rangle - \langle U_S\rangle^2] = 4\left[\int_{\mathbb{R}} dy\; w_S(x-x'+y)w_S(y)\right]^2. \tag{38}$$

Contrarily to choice (31), w_S should not be normalized to unity here because—from Eq. (36)—this is homogeneitywise impossible. Instead, the choice

$$w_S(x) = \left(\frac{\ell_c}{4\pi^3}\right)^{1/4}\frac{\sin\left(\frac{x}{\ell_c}\right)}{x} \tag{39}$$

corresponds to the typical experimental situations [42] and leads to a correlation function

$$C_S(x) = \frac{\ell_c}{\pi}\frac{\sin^2\left(\frac{x}{\ell_c}\right)}{x^2}, \tag{40}$$

whose integral over x equals unity and whose Fourier transform is

$$\hat{C}_S(q) = \begin{cases} 1 - |q|\ell_c/2 & \text{if } |q|\ell_c < 2 \\ 0, & \text{otherwise.} \end{cases} \tag{41}$$

Hence, definition (36) and choice (39) correspond here also to characterizing the amplitude of the disorder's fluctuations by the parameter σ and the range of the correlations by ℓ_c.

V. SUPERSONIC STATIONARY REGIME

As explained in Ref. [14], and recalled in the Introduction, Anderson localization in a weakly repulsive Bose-Einstein condensate is only possible in the supersonic regime (cf. Fig. 1), which we consider now. In the present section we first analyze the transmission across a short disordered sample, in which case perturbation theory is applicable (Sec. V A). We then turn to generic nonperturbative configurations (Sec. V B) where Anderson localization is expected. In this regime we obtain evidences of the occurrence of Anderson localization in the presence of interaction. Finally, we discuss the upper limit of the localized regime and the onset of time-dependent flows for long disordered samples (Sec. V C).

A. Perturbation theory ($\lambda \ll 1$)

In the supersonic stationary regime, simple perturbation theory yields $n(x,t) = n_0 + \delta n(X)$, where [22]

$$\delta n(X) = \frac{2mn_0}{\hbar^2\kappa}\int_{-\infty}^{X} dy\ U(y)\sin[2\kappa(X-y)] \tag{42}$$

and κ is given by Eq. (14). Perturbation theory always predicts a stationary density profile. This is certainly wrong when V is close to c (cf. Fig. 1), but in this case κ gets very small and one precisely goes out of the domain of validity of perturbation theory [δn as given by Eq. (42) is no longer small compared to n_0].

Far ahead of the obstacle (in a region where $X-L$ is larger than ℓ_c and κ^{-1}), Eq. (42) gives

$$\frac{\delta n(X)}{n_0} = \frac{2m}{\hbar^2\kappa}\mathrm{Im}\{e^{2i\kappa X}\hat{U}(2\kappa)\}. \tag{43}$$

The perturbative regime in which Eqs. (42) and (43) are valid is also the one where the constant λ in Eqs. (16) and (17) is small compared to unity. This can be inferred from the comparison of Eqs. (17) and (43) which indeed shows that $\lambda \ll 1$ in the regime where Eq. (43) holds and that, in this case, $\sqrt{\lambda} \simeq m|\hat{U}(2\kappa)|/(\hbar^2\kappa)$. The corresponding reflection coefficient can then be obtained from Eq. (20), yielding

$$R \simeq \lambda \simeq \frac{m^2}{\hbar^4\kappa^2}|\hat{U}(2\kappa)|^2. \tag{44}$$

From Eq. (44) it is clear that the average reflection coefficient is

$$\langle R\rangle = \langle\lambda\rangle = \frac{m^2}{\hbar^4\kappa^2}\langle|\hat{U}(2\kappa)|^2\rangle \ll 1. \tag{45}$$

Furthermore, one can show that the corresponding probability distribution of the reflection coefficient is Poissonian with

$$P(R) = \frac{1}{\langle R\rangle}\exp(-R/\langle R\rangle). \tag{46}$$

Note that, for properly normalizing this probability distribution for $R\in[0,1]$, one should include in the prefactor of the r.h.s. of Eq. (46) a correcting term of order $\exp(-1/\langle R\rangle)$, which can be safely neglected in the limit (45).

We give in Appendix A a demonstration of result (46) for the special case of a correlated Gaussian potential U_g of type (25). Below, we show that the same result holds for a potential U_δ of type (21) [see Eq. (68) in Sec. V B], and we checked numerically that it is also the case for the speckle potential U_S (36) (cf. Fig. 4). In all these cases, the average reflection coefficient reads (up to the above discussed exponentially small correction)

$$\langle R\rangle = L/L_{\mathrm{loc}}(\kappa), \tag{47}$$

where

$$L_{\mathrm{loc}}(\kappa) = \frac{\kappa^2/\sigma}{\hat{C}(2\kappa)}. \tag{48}$$

We recall that the function $\hat{C}$ depends on the type of disorder considered. For a potential of form (21), one has $\hat{C}_\delta \equiv 1$; for the other potentials considered in this work it is given by Eqs. (34), (35), and (41).

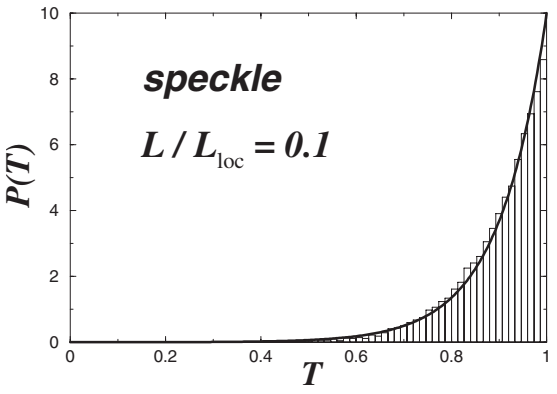

FIG. 4. Probability distribution $P(T)$ for the transmission coefficient T in a potential U_S with $\sigma=3.14\mu^2\xi$, $\ell_c=0.1\xi$, and $L=50\xi$ moving at velocity $V=7c$ in a condensate of initial constant density $n_0\xi=1$. The corresponding localization length is $L_{\mathrm{loc}}=500\xi$. The histogram corresponds to a statistical analysis of the results of the numerical solution of Eq. (1) for 10 000 different random potentials. The solid line is the perturbative result (49).

Concomitantly to distribution (46) of reflection coefficients, one gets for the transmission

$$P(T) = \frac{L_{\mathrm{loc}}}{L}\exp\left\{-(1-T)\frac{L_{\mathrm{loc}}}{L}\right\}. \tag{49}$$

From Eq. (49) [or Eq. (47)], one gets

$$\langle T\rangle = 1 - \frac{L}{L_{\mathrm{loc}}(\kappa)}. \tag{50}$$

The perturbative approach holds when $\langle R\rangle \ll 1$, i.e., when $L \ll L_{\mathrm{loc}}$. This corresponds to the region which is denoted as "ballistic" in Fig. 1 [45]. Its accuracy is shown for $L/L_{\mathrm{loc}}=0.1$ in Fig. 4 for a speckle potential U_S of type (36) (we also checked this prediction for the potentials U_δ and U_G, with also excellent results).

At this stage, L_{loc} is simply a notation for expression (48), but it will be shown to be the actual localization length of the matter wave in a disordered potential (in Sec. V B).

The results derived here also hold for a noninteracting gas, obtained by taking the limit $g\to 0$ in Eq. (1), in which case $c=0$ and $\kappa=k$. Equation (48), with κ replaced with k, then coincides with the Antsygina-Pastur-Slyusarev formula for the localization length [46,47] and the distribution of transmissions (49) holds, with $L_{\mathrm{loc}}=L_{\mathrm{loc}}(k)$.

In the present work, those formulas are modified to include interactions. The generalization simply consists in replacing the wave vector $k=mV/\hbar$ with $\kappa=m(V^2-c^2)^{1/2}/\hbar$. This replacement has—as an important physical consequence—the effect of diminishing, at a given speed V, the localization length (there is an effective reduction of the available kinetic energy by the repulsive interactions). For instance, in the case of a potential U_δ, since $L_{\mathrm{loc}}(\kappa)\propto\kappa^2$, there is a relative difference c^2/V^2 between $L_{\mathrm{loc}}(\kappa)$ and $L_{\mathrm{loc}}(k)$, that is 11% for $V=3c$. This is illustrated in Fig. 5, which displays the average $\langle T\rangle$ as a function of L for a disorder U_δ of type (21), with and without interactions.

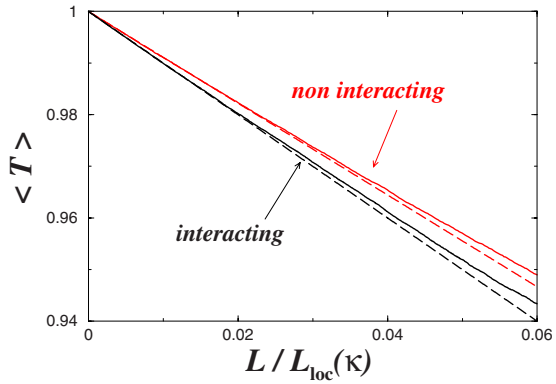

FIG. 5. (Color online) Average transmission as a function of L for a potential U_δ (characterized by $n_\delta\xi=0.5$ and $\xi/b=0.1$). In the interacting case $V=3c$ and $L_{\rm loc}(\kappa)=1600\xi$. The noninteracting case is drawn for the same velocity and corresponds to a value $L_{\rm loc}(k)=\frac{9}{8}L_{\rm loc}(\kappa)=1800\xi$. In both cases the dashed line is the analytical result (50) and the solid line corresponds to a statistical analysis of the results of the numerical solution of Eq. (1) for 15 000 different random potentials. The departure of the numerical results from the dashed lines occurs when the systems leaves the perturbative regime.

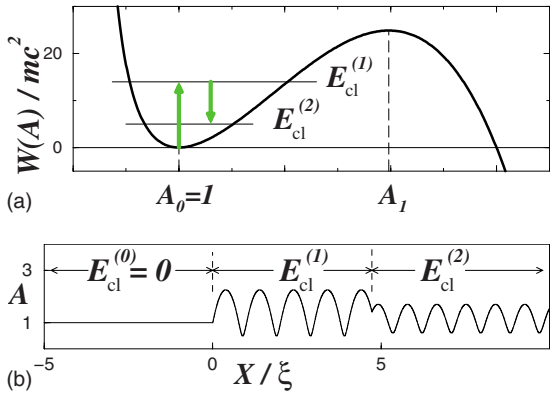

FIG. 6. (Color online) Upper panel: W as a function of A (drawn for $V/c=4$). For $X<x_1=0$, the fictitious particle is initially at rest at the bottom of potential W with $E_{\rm cl}^{(0)}=0$. The value of the classical energy changes from $E_{\rm cl}^{(n-1)}$ to $E_{\rm cl}^{(n)}$ at each impurity x_n. The lower panel displays the corresponding oscillations of $A(X)$, with two impurities at $x_1=0$ and $x_2=4.7\xi$ (their position is indicated by vertical dashed lines).

B. Nonperturbative approach

When the size L of the sample is large compared to the value $L_{\rm loc}$ determined in Sec. V A, the perturbative approach fails. We now propose a nonperturbative method allowing to treat both the regimes $L<L_{\rm loc}$ and $L\geq L_{\rm loc}$ and showing that $L_{\rm loc}$, as defined in Eq. (48), is indeed the localization length in the presence of interactions.

Within the framework of the nonperturbative approach, we are able to provide approximate analytical results in the case of the model disorder potential (21). This potential being zero between two impurities, one can write a series of first integrals of Eq. (5) in each segment $]x_n,x_{n+1}[$ as follows:

$$\frac{\hbar^2}{2m}\left(\frac{dA}{dX}\right)^2+W[A(X)]=E_{\rm cl}^{(n)}. \tag{51}$$

In the region $X<x_1=0$ the integration constant $E_{\rm cl}^-$ of Eq. (7) is denoted as $E_{\rm cl}^{(0)}$ in Eq. (51) (taking $x_0=-\infty$) and is zero, whereas in the region $X>x_N$ one has $E_{\rm cl}^+=E_{\rm cl}^{(N)}$ (and $x_{N+1}=+\infty$).

From Eq. (5) it is a simple matter to show that the matching condition of the density at impurity position x_n is

$$A'(x_n^+)-A'(x_n^-)=\frac{2}{b}A(x_n), \tag{52}$$

where $A'(x_n^-)$ $[A'(x_n^+)]$ denotes the limit of the derivative dA/dX at the left [at the right] of x_n. Relation (52) between the derivatives of the amplitude results [from Eq. (51)] in a relation between the classical energies,

$$E_{\rm cl}^{(n)}=E_{\rm cl}^{(n-1)}+\frac{2\hbar^2}{mb^2}A(x_n)[bA'(x_n^-)+A(x_n)]. \tag{53}$$

Hence, Eq. (51) allows one to draw a classical analog of the solution of the nonlinear Schrödinger equation in the presence of potential (21) formed by a series of delta peaks: the fictitious classical particle defined in Sec. III B evolves in the potential W and experiences kicks at times x_n. Each kick changes the "energy" according to Eq. (53), as illustrated in Fig. 6. The key point in the remaining of this section will be to derive the probability distribution of $E_{\rm cl}^+=E_{\rm cl}^{(N)}$ which then directly allows one to get the distribution of λ's and of the transmission coefficients [through Eqs. (16) and (20)].

Let us introduce the quantities

$$\lambda_n=\frac{mE_{\rm cl}^{(n)}}{2\hbar^2\kappa^2},\quad \Lambda_n=\sqrt{(\lambda_n)^2+\lambda_n}. \tag{54}$$

The parameters λ and Λ defined in Eqs. (16) and (18) are related to the ones of Eq. (54) by $\lambda=\lambda_N$ and $\Lambda=\Lambda_N$ (i.e., λ is the last of λ_n's; the same holds for Λ). Denoting by θ_{n-1} the value of the phase θ [appearing in Eq. (17)] for $X\in]x_{n-1},x_n[$, one gets in this domain [the derivation is exactly the same as for Eq. (17)]

$$A^2(X)=1+2\lambda_{n-1}+2\Lambda_{n-1}\cos(2\kappa X+\theta_{n-1}), \tag{55}$$

and one can rewrite Eq. (53) as

$$E_{\rm cl}^{(n)}=E_{\rm cl}^{(n-1)}+\frac{2\hbar^2}{mb^2}[1+2\lambda_{n-1}]+\frac{4\hbar^2}{mb^2}\Lambda_{n-1}\sqrt{\kappa^2b^2+1}\zeta_{n-1}, \tag{56}$$

where

$$\zeta_{n-1}=\cos[2\kappa x_n+\theta_{n-1}+\tan^{-1}(\kappa b)]. \tag{57}$$

Using definition (54) one can rewrite Eq. (56) in terms of the parameter λ_n as

$$\lambda_n=\lambda_{n-1}+\frac{1+2\lambda_{n-1}}{\kappa^2b^2}+\frac{2\Lambda_{n-1}}{\kappa^2b^2}\sqrt{\kappa^2b^2+1}\zeta_{n-1}. \tag{58}$$

Equations (56) and (58) are valid provided Eq. (11) holds, i.e., provided $E_{\rm cl}^{(n-1)}\ll W(A_1)$, which reads

$$E_{\mathrm{cl}}^{(n-1)} \ll \frac{\hbar^2\kappa^2}{m}(\kappa^2\xi^2), \quad \text{i.e.,} \quad \lambda_{n-1} \ll \kappa^2\xi^2. \tag{59}$$

In the following we also impose the condition

$$\kappa b \gg 1. \tag{60}$$

Precisely, we neglect all the quantities of order $1/(\kappa^3 b^3)$. This is an important technical point. It facilitates the analysis by allowing one to get simple formulas as we now illustrate in the perturbative case: Eq. (58) allows, for instance, to compute the average value of the reflection coefficient in the perturbative regime [as already done in Sec. V A, Eq. (47)]. In this regime, additionally to condition (59) one has $\lambda_n \ll 1$. Then Eq. (58) implies at leading order $\langle\lambda_n\rangle = \langle\lambda_{n-1}\rangle + 1/(\kappa^2 b^2)$ which, together with the initial condition $\lambda_0 = 0$, leads immediately to

$$\langle\lambda\rangle = \frac{1}{\kappa^2 b^2}\langle N\rangle = \frac{1}{\kappa^2 b^2}\frac{L}{l_\delta}, \tag{61}$$

which is identical to result (47) in the case of a potential U_δ for which $L_{\mathrm{loc}}(\kappa) = \kappa^2/\sigma = \kappa^2 b^2 l_\delta$ [cf. Eq. (48)].

Let us now proceed and consider the generic nonperturbative regime where λ_n may become large compared to unity and where Eqs. (11) and (59) are still valid. Taking condition (60) into account, Eq. (58) reads

$$\lambda_n = \lambda_{n-1} + \frac{1+2\lambda_{n-1}}{\kappa^2 b^2} + \frac{2\Lambda_{n-1}}{\kappa b}\zeta_{n-1}. \tag{62}$$

It is natural to assume that the phase of the cosine in the r.h.s. of Eq. (57) is uniformly distributed in $[-\pi, \pi]$ and independent of the phase at step $n-1$. This could be called a "phase randomization" approximation. This relies on hypothesis (60) and on the assumption that there is a large number of density oscillations over the (random) length between x_{n-1} and x_n, i.e.,

$$\kappa\langle x_n - x_{n-1}\rangle = \kappa l_\delta \gg 1. \tag{63}$$

Then, the argument of the cosine in definition (57) is uniformly distributed; ζ_n's are uncorrelated random variables, with all the same law characterized by its average $\langle\zeta_n\rangle = 0$ and variance

$$\langle\zeta_n\zeta_{n'}\rangle = \tfrac{1}{2}\delta_{n,n'}. \tag{64}$$

Note that the regimes (60) and (63) imply that

$$\frac{\hbar^2\kappa^2}{2m} \gg \frac{\hbar^2 n_\delta}{mb} = \langle U_\delta\rangle, \tag{65}$$

which in turn implies that the kinetic energy $\frac{1}{2}mV^2$ is much larger than $\langle U_\delta\rangle$; i.e., one is exactly in the Anderson regime where the incident kinetic energy is much larger than the typical value of the (disordered) potential representing the obstacle. Hence, a classical particle would flow almost unperturbed over the potential but, as we shall see, a quantum particle experiences an exponentially small transmission.

Let $P(\lambda, n)d\lambda$ be the probability that λ_n lies in the interval λ, $\lambda + d\lambda$. Going to the continuous limit and defining the continuous variable $t = n/(\kappa^2 b^2) = X/L_{\mathrm{loc}}$ [where $L_{\mathrm{loc}} = \kappa^2/\sigma$ is the parameter (48) in the case of a potential U_δ] it is shown in Appendix B that $P(\lambda, t)$ verifies the following Fokker-Planck equation:

$$\frac{\partial P}{\partial t} = \frac{\partial}{\partial\lambda}\left[\lambda(1+\lambda)\frac{\partial P}{\partial\lambda}\right]. \tag{66}$$

Equation (66) follows directly from Eq. (62) in the regime where conditions (60) and (63) hold. It is precisely the Dorokhov-Mello-Pereyra-Kumar (DMPK) equation [48] for the transmission in a single disordered channel [with $T = 1/(1+\lambda)$]. Equation (66) is sometimes referred to as Mel'nikov's equation (after Ref. [49]) but has a much longer history (see the discussion in Refs. [47,50]).

Since before entering the disordered region the particle has a classical energy $E_{\mathrm{cl}}^{(0)} = 0$ corresponding to $\lambda = 0$, Eq. (66) has to be solved for the initial condition

$$\lim_{t\to 0} P(\lambda, t) = \delta_+(\lambda), \tag{67}$$

where δ_+ is the one-sided delta function: $\int_0^\infty \delta_+(\lambda)d\lambda = 1$. In the limit of small t (i.e., in the perturbative regime $X \ll L_{\mathrm{loc}}$), λ remains small and one can approximate in the r.h.s. of Eq. (66) the term $\lambda(\lambda+1)$ by λ. It is then simple to verify that the solution of this approximate equation that satisfies Eq. (67) is

$$P(\lambda, t) = \frac{\exp\{-\lambda/t\}}{t} \quad \text{for} \quad t \ll 1. \tag{68}$$

This result for the small t solution of the DMPK equation has been already obtained in Ref. [51] (see also the discussion in Ref. [52]). The distribution law (68) is exactly equivalent to distribution (46) of the reflection coefficient in the perturbative regime and this proves the validity of the Poissonian distribution (49) for a potential U_δ of type (21) [53].

In the general case (i.e., for all $t \geq 0$) the solution of Eq. (66) with the initial condition (67) is (see, e.g., Refs. [47,50] and references therein)

$$P(\lambda, t) = \frac{e^{-t/4}}{\sqrt{2\pi t^3}}\int_{u_\lambda}^\infty \frac{u e^{-u^2/(4t)}}{\sqrt{\cosh(u) - 1 - 2\lambda}}du, \tag{69}$$

where $u_\lambda = \cosh^{-1}(1+2\lambda)$.

From distribution (69), a lengthy computation or alternatively the direct use of the DMPK equation (66) [54] yields

$$\langle\ln T\rangle = \int_0^\infty d\lambda\, \ln\left(\frac{1}{1+\lambda}\right)P(\lambda, t) = -t. \tag{70}$$

In the large t limit, distribution (69) tends to a log-normal distribution, i.e., the distribution of the variable $\ln T$ is Gaussian (see Ref. [54])

$$P(\ln T, t) = \frac{\exp\{-(t+\ln T)^2/4t\}}{\sqrt{4\pi t}} \quad \text{for} \quad t \gg 1. \tag{71}$$

From this distribution one gets the correct average $\langle\ln T\rangle = -t$ [Eq. (70)] and a standard deviation $[\langle(\ln T)^2\rangle - \langle\ln T\rangle^2]^{1/2} = \sqrt{2t}$, which is in agreement with the exact result in the limit $t \gg 1$ [54]. At the extremity of a sample of length L, one has $t = L/L_{\mathrm{loc}}$, and distribution (71) is the logarithmic-normal distribution of transmission typical for Anderson localization in the regime $L \gg L_{\mathrm{loc}}$ (see, e.g., Refs. [50,55]). As

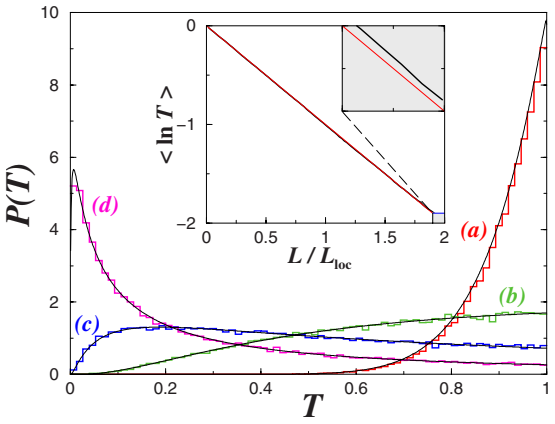

FIG. 7. (Color online) Probability distribution of the transmission through a disordered potential U_δ of type (21) (characterized by $\xi/b=0.5$ and $n_\delta\xi=0.5$) plotted for different values of the ratio $t=L/L_{\rm loc}(\kappa)$ with $V=30c$. The black solid lines are the DMPK result (69) and the colored histograms correspond to the numerical simulations (50 000 samples used for each value of t). Cases (a), (b), (c), and (d) correspond, respectively, to $t=0.1$, 0.5, 1, and 2. The inset displays $\langle \ln T\rangle$ as a function of t. The thick solid line is extracted from numerical simulations and the thin (red) solid line is the DMPK prediction (70). They can be distinguished only around $t\simeq 2$ as shown in the blowup of the (gray) shaded region for $1.9<t<2$.

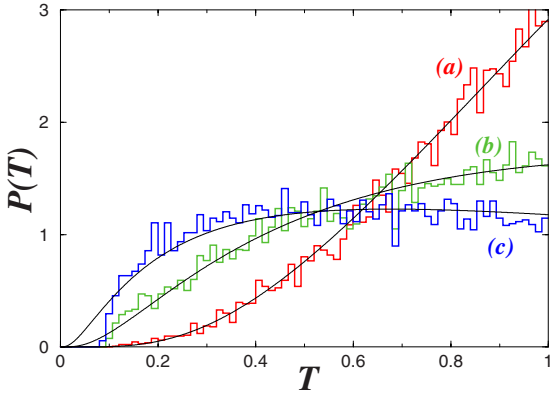

FIG. 8. (Color online) Probability distribution of the transmission through a speckle disordered potential U_S (characterized by $\ell_c/\xi=0.05$ and $\sigma=3.13\mu^2\xi$) plotted for different values of the ratio $t=L/L_{\rm loc}(\kappa)$ with $V=13c$. Curves (a), (b), and (c) corresponds, respectively, to $t=0.31$, 0.52, and 0.68. For each curve, the black solid line is the DMPK result (69) and the colored histogram is the result of 10 000 numerical simulations.

a side product of this analysis, Eqs. (70) and (71) confirm that $L_{\rm loc}$ is indeed the localization length as was anticipated in the notation.

We have tested the validity of the DMPK approach for a Bose-Einstein beam of interacting particles propagating in a disordered potential U_δ of type (21). The numerical results for the probability distribution $P(T)$ are compared in Fig. 7 with the DMPK prediction (69). The agreement is seen to be excellent. The distribution evolves from the Poissonian result (49) (for low values of $L/L_{\rm loc}$) toward a distribution peaked at low-T values for large $L/L_{\rm loc}$. In this latter case one can check that the distribution tends to a log-normal by plotting $P(\ln T)$.

We have also checked the validity of the present approach over a sizable range of lengths of disordered region and of intensities of disordered potential by plotting in the inset of Fig. 7 the average $\langle \ln T\rangle$ as a function of $L/L_{\rm loc}$. The agreement of the numerical results with the DMPK prediction (70) is excellent. Note however the beginning of a small departure around $L/L_{\rm loc}\simeq 2$; this effect will be studied more thoroughly in Sec. V C (cf. Fig. 9).

Finally, we discuss numerical results obtained for the disordered potentials introduced in Secs. IV B and IV C. Although we do not have an analytical derivation of the DMPK equation for these potentials, the numerical results indicate a very good quantitative agreement for a disordered potential U_G and for a speckle potential U_S. We display the comparison of the numerical data with the DMPK predictions for a speckle potential in Fig. 8. The same agreement is obtained for a Gaussian potential U_G. Hence, the behavior analytically predicted for the potential U_δ appears to be of general validity, meaning that the above defined regime of phase randomization can probably be extended to correlated potentials, leading to a regime of single parameter scaling. However, we have noticed that, although showing an overall good agreement with the DMPK prediction, the Lorentzian correlated potential U_L exhibits some deviations in the tail of the distribution; the details of which will be studied elsewhere.

C. Threshold for the existence of a stationary flow

In the previous sections the main effect of interaction has been shown to be a renormalization of the localization length $L_{\rm loc}$. Interaction induces a modification of the wave vector: expression (48) for the localization length coincides with the noninteracting one but computed for an effective interaction-dependent wave vector κ given by Eq. (14), instead of $k=mV/\hbar$. The repulsive interaction diminishes the available kinetic energy and therefore reduces the localization length with respect to the noninteracting case (since $\kappa<k$).

We now discuss another, more spectacular, effect of interactions on the localization properties of a propagating BEC on a disordered potential. In the previous Secs. V A and V B, we completely neglected the presence of an upper limit for the classical energy $E_{\rm cl}$, which is given by the local maximum of the effective potential $W(A)$, namely, $E_{\rm cl}^{\rm max}=W(A_1)$ (see Fig. 3). Trajectories that pass beyond $E_{\rm cl}^{\rm max}$ would become unstable and develop singularities with infinitely large density at $X\to\infty$. In practice this implies, on the level of Eq. (1), that a stationary flow cannot be maintained in this case and that the disorder induces time-dependent dynamics of the condensate.

In the vicinity of $E_{\rm cl}^{\rm max}$, the density profile of the condensate in between two adjacent scatterers becomes quite different from the cosine shape (17) that was derived for weak nonlinearities and/or low density modulations and resembles more to a periodic train of gray solitons [22]. In a crude approximation, we neglect this complication and assume that the spatial evolution of the density is still given by Eq. (17) for all classical energies until $E_{\rm cl}=E_{\rm cl}^{\rm max}$. Trajectories that happen to pass beyond $E_{\rm cl}^{\rm max}$ are considered to be "lost," i.e.,

they do no longer contribute to the probability distribution for the transmission. This formally amounts to introducing a "sink" in the stochastic equation (62), namely, at $\lambda=\lambda_{\max}=mE_{\rm cl}^{\max}/(2\hbar^2\kappa^2)$. In the corresponding Fokker-Planck equation (66), this sink is appropriately modeled by imposing the boundary condition

$$P(\lambda_{\max},t)=0. \tag{72}$$

As a consequence of this boundary condition, the integrated probability distribution $\int_0^{\lambda_{\max}}P(\lambda,t)d\lambda$ is no longer conserved, but decreases with increasing t, i.e., increasing length L of the disorder region.

In the following, we show how this affects the DMPK predictions of Sec. V B and how the "survival probability," i.e., the fraction of trajectories that remain below this boundary at given length L, can be analytically computed in the limit $V\gg c$. In this limit, from Eq. (10) one gets $E_{\rm cl}^{\max}\simeq mV^4/(8c^2)$ and thus $\lambda_{\max}\simeq V^2/(16c^2)\gg 1$. Modifications of the probability density $P(\lambda,t)$ due to the presence of the sink appear only when the typical value of λ is of order $\lambda_{\max}$ which, as just remarked, is large compared to unity in the case $V\gg c$. In this case $P(\lambda,t)$ is already negligibly small around $\lambda\sim 1$. We therefore make the approximation $\lambda+1\simeq\lambda$ in the Fokker-Planck equation (66), which then reads

$$\frac{\partial P}{\partial t}=\frac{\partial}{\partial\lambda}\left[\lambda^2\frac{\partial P}{\partial\lambda}\right]. \tag{73}$$

Using, from now on, the probability distribution $P(\ln T,t)$ for finding a given value of $\ln T$ at fixed $t\equiv L/L_{\rm loc}$, we obtain in this limit

$$\frac{\partial}{\partial t}P(z,t)=\frac{\partial^2}{\partial z^2}P(z,t)-\frac{\partial}{\partial z}P(z,t), \tag{74}$$

where we introduce $z\equiv-\ln T$. Clearly, the log-normal distribution (71) corresponds to a solution of Eq. (74) in the absence of any additional boundaries.

In the presence of the sink, which is imposed by the boundary condition $P(z_{\max},t)=0$ with

$$z_{\max}=\ln(\lambda_{\max}+1)\simeq\ln\lambda_{\max}\simeq\ln\left(\frac{V^2}{16c^2}\right), \tag{75}$$

we can straightforwardly find the solution of Eq. (74) by subtracting from the log-normal distribution (71) a "mirror" distribution centered at some $z>z_{\max}$ (namely, $2z_{\max}+t$) with a suitable prefactor. This yields the distribution

$$P(z,t)=\frac{1}{\sqrt{4\pi t}}\left[\exp\left(-\frac{(z-t)^2}{4t}\right)-e^{z_{\max}}\times\exp\left(-\frac{(z-t-2z_{\max})^2}{4t}\right)\right], \tag{76}$$

which is defined for $z<z_{\max}$. Clearly, this distribution satisfies the evolution equation (74) as well as the boundary condition $P(z_{\max},t)=0$ for all t and the initial condition $P(z,0)=\delta(z)$ for $z<z_{\max}$.

The presence of the sink at $z=z_{\max}$ explains a phenomenon barely noticeable in Fig. 7, but exemplified in Fig. 9, namely, the departure of the observed average $\langle\ln T\rangle$ from the usual DMPK result $\langle\ln T\rangle=-t$. This departure is due to the fact that the numerically computed average only takes into account the stationary solutions which—as will be seen from Eq. (79)—become less and less numerous when t increases. Hence, what is computed numerically is the average of $\ln T=-z$ over distribution (76). This reads

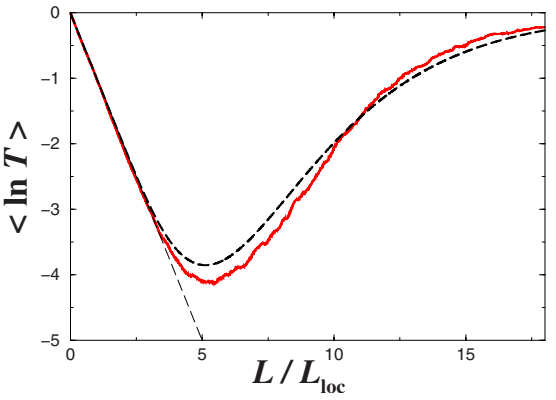

FIG. 9. (Color online) $\langle\ln T\rangle=-\langle z\rangle$ plotted as a function of $t=L/L_{\rm loc}(\kappa)$ in the case of random potentials U_δ characterized by $n_\delta\xi=0.5$ and $\xi/b=\sqrt{2}$. The curve is drawn in the case $V/c=450$. The red solid line is the numerical result and the black dashed line is the analytical result (77). The straight (thin dashed) line is the usual DMPK result $\langle\ln T\rangle=-t$ [Eq. (70)].

$$\begin{aligned}\langle z\rangle&=\int_{-\infty}^{z_{\max}}zP(z,t)dz\\&=\frac{t}{2}\left[1+\mathrm{erf}\left(\frac{z_{\max}-t}{2\sqrt{t}}\right)\right]\\&\quad-e^{z_{\max}}\left(\frac{t}{2}+z_{\max}\right)\mathrm{erfc}\left(\frac{t+z_{\max}}{2\sqrt{t}}\right).\end{aligned} \tag{77}$$

where the error function is defined by

$$\mathrm{erf}(x)=\frac{2}{\sqrt{\pi}}\int_0^x\exp(-y^2)dy, \tag{78}$$

and $\mathrm{erfc}(x)=1-\mathrm{erf}(x)$.

Expression (77) is compared in Fig. 9 with the results of a numerical simulation performed in the case $V/c=450$ (corresponding to $z_{\max}=9.43$) for 10 000 random potentials U_δ of type (21) characterized by $n_\delta\xi=0.5$ and $\xi/b=\sqrt{2}$ [leading to $L_{\rm loc}(\kappa)=100\xi$]. The agreement is seen to be very good. Since the sink cuts the solutions which are strongly scattered by the random potential, the remaining stationary states have a higher transmission coefficient. This effect increases with the sample length L, which explains the behavior of the curve in Fig. 9.

As another test of the validity of our approach (which amounts to model the upper boundary $z_{\max}$ by a perfect sink and to neglect nonlinear deformations of the density pattern of the flow close to the threshold), we now determine the probability for a trajectory to remain below the boundary. This survival probability reads

$$P_s(t) = \int_{-\infty}^{z_{\max}} P(z,t)dz$$
$$= \frac{1}{2}\left[1 + \mathrm{erf}\left(\frac{z_{\max} - t}{\sqrt{4t}}\right)\right] - \frac{e^{z_{\max}}}{2}\mathrm{erfc}\left(\frac{z_{\max} + t}{\sqrt{4t}}\right). \tag{79}$$

As anticipated, $P_s(t)$ clearly decreases from 1 (at $t=0$) to 0 (for large t). The knowledge of $P_s(t)$ allows one to determine the value L^* of the length of the disordered region beyond which most of the random realizations lead to a nonstationary flow of the condensate. We can, most conveniently, define L^* through the condition

$$P_s(t^*) = 1/2, \tag{80}$$

with $t^* \equiv L^*/L_{\mathrm{loc}}$. This leads to the implicit equation for the threshold value t^*,

$$\mathrm{erf}\left(\frac{z_{\max} - t^*}{\sqrt{4t^*}}\right) = e^{z_{\max}}\,\mathrm{erfc}\left(\frac{z_{\max} + t^*}{\sqrt{4t^*}}\right). \tag{81}$$

This equation can be explicitly solved in the limiting case of large $z_{\max}$. As it is natural to assume that t^* ought to be of the order of $z_{\max}$, which is the only relevant scale in this equation, we make the ansatz

$$t^* = z_{\max} + \delta t \tag{82}$$

and assume (which is to be verified *a posteriori*) that δt is of the order of unity, whereas $z_{\max} \gg 1$. This yields to lowest nonvanishing order

$$\mathrm{erf}\left(\frac{z_{\max} - t^*}{\sqrt{4t^*}}\right) = -\frac{\delta t}{\sqrt{\pi z_{\max}}}[1 + O(z_{\max}^{-1})], \tag{83}$$

for the left-hand side of Eq. (81) and

$$e^{z_{\max}}\,\mathrm{erfc}\left(\frac{z_{\max} + t^*}{\sqrt{4t^*}}\right) = e^{z_{\max}}\frac{2}{\sqrt{\pi}}\int_{\sqrt{z_{\max}}}^{\infty} e^{-y^2}dy[1 + O(z_{\max}^{-2})]$$
$$= \frac{1}{\sqrt{\pi z_{\max}}}[1 + O(z_{\max}^{-1})], \tag{84}$$

for the right-hand side of Eq. (81). This finally results in

$$\delta t = -1 + O(z_{\max}^{-1}). \tag{85}$$

Neglecting terms of the order of $z_{\max}^{-1}$, we therefore obtain for the threshold length

$$L^* = (z_{\max} - 1)L_{\mathrm{loc}} = L_{\mathrm{loc}}\left[\ln\left(\frac{V^2}{16c^2}\right) - 1\right]. \tag{86}$$

We emphasize that Eq. (86) holds for $z_{\max} \gg 1$, i.e., for $\ln(V^2/16c^2) \gg 1$ [see Eq. (75)]. This is much more restrictive than the condition $V \gg c$ which is assumed to hold true when deriving Eqs. (76) and (81).

Figure 10 shows a comparison of the analytical predictions (79) and (86) with numerical data obtained from the integration of the time-dependent Gross-Pitaevskii equation (1). The condensate flows through a disorder potential U_δ of type (21) with $V^2/c^2 = 2\times 10^5$. We see that the fraction of stationary trajectories $P_s(t)$ is very well described by Eq. (79), and that the approximate expression (86) predicts very well the length L^* at which the crossover length from stationary to time-dependent flow occurs.

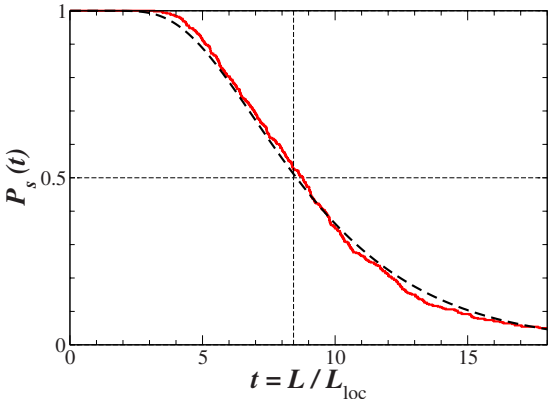

FIG. 10. (Color online) Fraction of stationary trajectories $P_s(t)$ plotted as a function of the length L of the disordered region. The condensate flow through disorder potentials U_δ of type (21) was numerically computed for this purpose (red solid line), at parameters for which $V^2/c^2 = 2\times 10^5$. The black dashed line shows the analytical prediction of this survival probability $P_s(L/L_{\mathrm{loc}})$ according to Eq. (79). The vertical dashed line marks prediction (86) for the threshold length L^* at which $P_s(L^*/L_{\mathrm{loc}}) = 1/2$ (horizontal dashed line), namely, $L^*/L_{\mathrm{loc}} = 8.433$.

For velocities V not extremely large compared to the speed of sound, the condition $z_{\max} \gg 1$ will not be fulfilled and estimate (86) will not be valid, while $\lambda_{\max} \gg 1$ might still hold and the average evolution of the system might still be fairly well described by the simplified Fokker-Planck equation (73). In that case, the implicit equation (81) has to be solved numerically. In Fig. 1 one can see that the numerical solution of Eq. (81) (yellow solid line) provides a very reasonable estimate of the boundary between the bright supersonic region (stationary flows) and the dark time-dependent region, in a regime of not extremely large V/c, where Eq. (86) fails to properly predict the threshold length L^*. The simulations are performed by solving Eq. (1) numerically using a potential of type U_δ (characterized by $\langle U_\delta\rangle/\mu = 0.025$ and $n_\delta \xi = 0.5$). For each V and L we consider 100 realizations of such a potential and statistically determine the quantity P_s, i.e., the fraction of stationary solutions. P_s is plotted in Fig. 1 using a grayscale (dark, $P_s = 0$; light blue/gray, $P_s = 1$) as a function of the normalized variables L/ξ and V/c (this normalization rescales interaction effects). The qualitative agreement of Fig. 1 is made quantitative in Fig. 11. In this figure the numerical solution of Eq. (81) is compared with its determination extracted from numerical simulations in the supersonic regime. More precisely, the solid (red) line in Fig. 11 is simply the contour $P_s = 1/2$ in Fig. 1. This corresponds exactly to definition (80) of L^*. The agreement between the numerical result and the theory of the present section [dashed curve, solution of Eq. (81)] is seen to be excellent [56].

We conclude this section by emphasizing that the existence of an upper threshold L^* corresponding to lengths of the disordered region beyond which most of the flows are

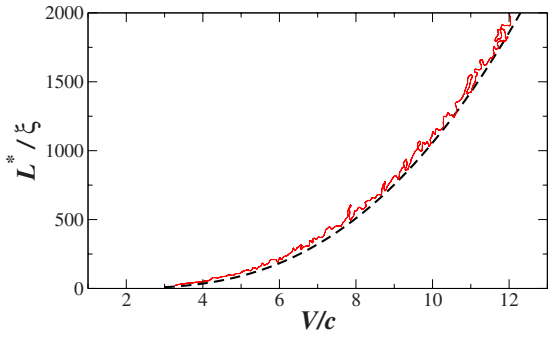

FIG. 11. (Color online) L^* as a function of V in dimensionless units. The black dashed line corresponds to the solution of Eq. (81) and the red solid line corresponds to the value of L^* extracted from numerical simulations for a potential U_δ with the same characteristics as in Fig. 1 (see the text).

time dependent is a genuine nonlinear effect [absent if one sets $g=0$ in Eq. (1)]. Actually, whereas interactions only weakly modify the precise value of the localization length, the existence of the threshold L^* is a remarkable qualitative effect induced by nonlinearity. Moreover, as illustrated in Figs. 9 and 10, this effect persists even in the limit $V \gg c$ where naively one would expect no noticeable consequence of interaction.

VI. EXPERIMENTAL CONSIDERATIONS

On the basis of the results obtained in the previous section we present here what are the more favorable experimental configurations for observing Anderson localization in an interacting Bose-Einstein beam. We also discuss a possible experimental signature of localization.

A. Appropriate configurations for observing Anderson localization

In the noninteracting regime the only condition for observing Anderson localization in one dimension is that the size of the disordered region should be larger than the localization length. Then one can observe an exponential decay of transmission with a log-normal distribution (in the limit $L \gg L_{\rm loc}$).

The situation is more complex when interactions are turned on. What is particularly interesting is the interplay between localization and superfluidity. Indeed these two phenomena are conflicting one with the other: superfluidity is the (counterintuitive) ability to pass over an obstacle without reflection, whereas Anderson localization corresponds to a large reflection in a domain where one would expect almost perfect transmission. As a result of the interplay between these two extreme phenomena, and depending on the fluid velocity and on the sample size, the flow may be stationary and superfluid, dissipative and time dependent, or stationary supersonic (and also dissipative) [14]. Anderson localization does not occur in the superfluid region (where the transmission is perfect) and either does not exist or cannot be clearly identified in the time-dependent regime (where interference effects are washed out [13]), but is truly observed in the supersonic stationary regime, as demonstrated in Sec. V.

In that regime, a first experimentally relevant effect is the modification of the localization length with respect to its value in the absence of interactions. This effect is very well described by renormalizing the wave vector k to κ [Eq. (48)], which means that part of the kinetic energy available to the flow is taken by interactions. However, as already discussed in Ref. [14] this effect is only sizable in a regime where V is not too large compared to c and is thus relevant only in the perturbative regime (cf. Fig. 5).

A second experimentally observable effect is the modification of the localization length due to the correlations of the disordered potential. This is described by formula (48) where $\hat{C}$ is the Fourier transform of the two-point correlation function of the disorder. For the different potentials considered here, $\hat{C} \equiv 1$ for a potential U_δ or is alternatively given by Eqs. (34), (35), and (41) for correlated potentials. Explicitly, this yields

$$L_{\rm loc}(\kappa) = \frac{\kappa^2}{\sigma}, \tag{87}$$

for a potential U_δ of type (21);

$$L_{\rm loc}(\kappa) = \frac{\kappa^2}{\sigma} \exp\{2\kappa^2 \ell_c^2\}, \tag{88}$$

for a potential U_G of type (25);

$$L_{\rm loc}(\kappa) = \frac{\kappa^2}{\sigma} \exp\{2\kappa \ell_c\}, \tag{89}$$

for a potential U_L of type (25); and

$$L_{\rm loc}(\kappa) = \frac{\kappa^2}{\sigma} \frac{1}{1-\kappa \ell_c}. \tag{90}$$

for a potential U_S of type (36) (when $\kappa \ell_c < 1$). The validity of these expressions has been tested in Sec. V B. In the noninteracting case (i.e., $\kappa = k$), expressions (87)–(90) correspond to a high-energy limit and can be obtained through a first-order Born expansion within the phase formalism of Refs. [46,47]. In all three cases, one sees that the localization length is drastically enhanced due to the nonzero correlation length with respect to the uncorrelated disorder [Eq. (87)]. In the Gaussian and the Lorentzian cases the localization length scales exponentially with $(\kappa \ell_c)^2$ and $\kappa \ell_c$, respectively [see Eqs. (88) and (89)]. In the case of a speckle potential, the effect is even stronger: one sometimes speaks of an "effective mobility edge" [57,58], meaning that beyond a critical wave vector (or a critical velocity) the localization length (90) is infinite. This is an artifact of the Antsygina-Pastur-Slyusarev formula (48), which can be corrected by going to higher orders (see Refs. [59–61]): the corrections to this result give a localization length which is finite, but typically larger than any other relevant scale in experimental systems.

Hence, in all the cases the dependence of the localization length with respect κ (i.e., with velocity) is amplified by correlations. Mathematically this is due to the fact that the denominator in the Antsygina-Pastur-Slyusarev formula (48) for the localization length in the presence of correlations

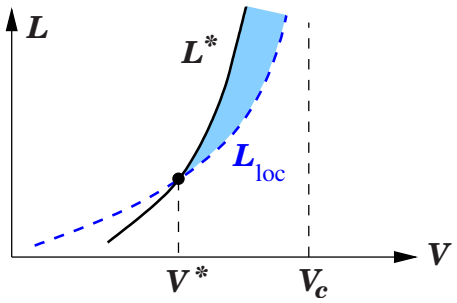

FIG. 12. (Color online) Schematic phase diagram in arbitrary units. The (blue) dashed line is the localization length $L_{\rm loc}$ and the solid line is the threshold length L^*. $V_c=\hbar/m\ell_c$ is the typical velocity beyond which it is almost impossible to observe Anderson localization in a realistic system (see text). The (blue) colored zone corresponds to the region where Anderson localization can be experimentally observed in presence of interaction.

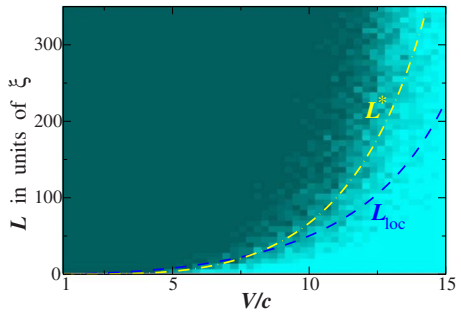

FIG. 13. (Color online) Phase diagram displaying the fraction of stationary trajectory P_s for a beam with velocity V moving in a speckle disorder of extent L. The figure has been drawn for a potential U_S of type (36) characterized by $\ell_c/\xi=0.05$ and $\sigma=3.93\mu^2\xi$. The light blue region corresponds to a domain of stationary flow ($P_s=1$: 100% of the solutions are stationary; see the explanation in the text); the dark region corresponds to time-dependent flow. The curves indicating the values of $L_{\rm loc}$ and L^* correspond to the analytical results (90)and to the numerical solution of Eq. (81).

tends to zero when $\kappa\ell_c \gg 1$. In order to minimize this effect one needs to impose the following condition:

$$\kappa\ell_c \lesssim 1 \quad \text{or} \quad V \lesssim V_c = \frac{\hbar}{m\ell_c} = c\frac{\xi}{\ell_c}. \tag{91}$$

In the r.h.s. of Eq. (91) we replaced κ with $mV/\hbar$ because in practice condition (91) is verified in regimes where $V \gtrsim 3c$, i.e., when the approximation $\kappa \simeq k$ is sound. Note that this condition is arbitrary and is only superficially analogous to the 3D Ioffe-Regel criterion [62]. The latter defines a true mobility edge that separates a metallic from a localized phase, whereas Eq. (91) only requires that the localization length does not get too large. Understood in this sense, criterion (91) is exactly equivalent to the definition of an effective mobility edge sometimes used in the literature.

In the absence of interactions it is always possible (at least theoretically) to define a system with a length $L > L_{\rm loc}$ which verifies Eq. (91); i.e., a system where one can observe Anderson localization. If we now turn on interactions, a major effect is the appearance of a length scale L^* which signals the onset, for $L > L^*$, of a regime of time-dependent flows (cf. Sec. V C). In this regime, Anderson localization disappears, and the time-averaged transmission coefficient scales as $1/L$ [13]. This is the most spectacular effect of interactions in the transport properties of the system. In order to observe Anderson localization, the system size should therefore satisfy $L_{\rm loc} < L < L^*$. In practice, one should be in a regime of parameters such as illustrated in Fig. 12: the crossing $L^* > L_{\rm oc}$ has to occur at a velocity lower than V_c.

Based on the numerical solution of Eq. (81) one can show that the crossing $L^* \geq L_{\rm loc}$ occurs at a velocity $V^* \simeq 7.95c$ [63] (see also Fig. 1). This condition only allows the system to reach a (stationary) regime where $L=L_{\rm loc}$. But if one wants to observe Anderson localization one should be able to reach a regime where, say, $L^* \gtrsim L \gtrsim 2L_{\rm loc}$, in order to get as close as possible to the domain of log-normal distribution of transmissions still remaining in the region of stationary flows. This imposes $V/c \gtrsim 20$. This must be supplemented by condition (91), i.e., $V/c \lesssim \xi/\ell_c$. Hence, the correlation length ℓ_c should be smaller or equal to $\xi/20$. Figure 13 shows the phase diagrams of a one-dimensional interacting beam of condensed atoms moving through a speckle potential in this regime. For plotting this diagram, one has generated 16 random potentials and studied in each case if a stationary solution exists or not. The dark blue region corresponds to a domain where no stationary solution exists while the light blue one corresponds to a domain where all the potentials admit a stationary solution (the color code is the same as in Fig. 1 and is explained in Sec. V C). The region between $L_{\rm loc}$ and L^* in Fig. 13 is the region where one can observe Anderson localization.

Let us now evaluate the orders of magnitude of the different parameters allowing one to reach the appropriate regime. For concreteness we consider a beam of ^{87}Rb atoms such as the one of the Atom Optics Group at Laboratoire Charles Fabry de l'Institut d'Optique. For a correlation length of 0.26 μm the velocity cutoff for observing Anderson localization is roughly $V_c \simeq 2.7$ mm/s. Note that in Ref. [2] the velocity of the expanding condensate is about 1.6 mm/s, i.e., smaller that V_c as it should. If we use the parameters of Ref. [64] ($an_1 \simeq 0.25$, $V \simeq 9$ mm/s, $a=5.3$ nm, $n_1=45$ atoms/μm, $c \simeq 0.9$ mm/s, and $\xi \simeq 0.8$ μm) it is impossible to satisfy condition (91) because $V \simeq 9$ mm/s $> V_c$ and also because $\ell_c/\xi \simeq 0.3$. However, the Atom Optics Group has recently improved the sensitivity of its detectors, which is now close to being able to detect a density as small as 1 atom/μm. This allows one to work with a smaller density and to improve the ratio ℓ_c/ξ, which can be tuned down to the value of 0.05. Then, the localization length can be selected by tuning the speckle amplitude. For instance $L_{\rm loc}=0.25$ mm can be obtained by choosing $\langle U_s \rangle = 34$ Hz at $V=1.6$ mm/s. These parameters are close to those used in Fig. 13 and are reachable experimentally. However, for observing Anderson localization one needs to keep the beam stable for almost 1 s (0.31 s if we want $L=2L_{\rm loc}$), whereas in the current experiment this is only possible during 0.1 s; hence, it is still a matter of debate to decide if the observation of Ander-

son localization of a Bose condensed beam in the presence of interaction is within the reach of present-time technology.

It is also interesting to make a connection between the physics described here and the recent experiment observation of Anderson localization of a condensate expanding in a disordered potential performed in the same group [2]. Contrarily to the propagation of a beam studied in the present work, Ref. [2] considers the spreading of a wave packet (initially at rest) in a speckle potential. After a first stage of expansion, mainly driven by interactions, the experimental cloud expands with a constant velocity $V \simeq 1.6$ mm/s but the particle density and the sound velocity are functions of the position. Therefore, it is not possible to place this experiment on a single point of the phase diagram displayed in Fig. 13. However one can evaluate the ratio V/c at different positions—that is, at different L. For instance, at the typical value $L = L_{\mathrm{loc}}$, Fig. 2 of Ref. [2] allows one to calculate the sound velocity as well as the healing length ξ, yielding the typical experimental values $V/c \simeq 12$ and $L/\xi \simeq 55$. Moreover, the ratio between the typical disorder amplitude $\langle U_S \rangle$ and the chemical potential $\mu = g n_0$ is the same in Fig. 13 and in experiment: $\langle U_S \rangle / \mu = 5$ (note however that in the experimental case this is the value of the *local* chemical potential that matters). Hence, although the experimental setup of Ref. [2] forbids a direct comparison with the results of the present work, the estimates of the typical values $V/c \simeq 12$ and $L/\xi \simeq 55$ indeed locate the experimental system within the regime of Anderson localization of Fig. 13.

B. Experimental signature

Once the appropriate regime of parameters for observing Anderson localization in a Bose condensed beam has been determined, it is also important to identify possible experimental signatures. In our theoretical approach we use the transmission coefficient T of the beam over the disordered region as the relevant parameter. However, the measure of T might be experimentally involved, and we propose here to use another related quantity, namely, the rate of energy dissipation [27] $\dot{E} = -V F_d$, where

$$F_d = \int_{\mathbb{R}} dx\, n(x,t) \frac{\partial U}{\partial x} \tag{92}$$

is the drag force exerted by the beam on the obstacle. Definition (92) is quite natural: the force exerted on the obstacle is the mean value of the operator $\partial_x U$ over the condensate wave function. It is rigorously justified by the analysis of Ref. [65] in terms of stress tensor. In the stationary case, changing integration from x to X in Eq. (92), a simple integration by parts yields

$$F_d = -n_0 \int_{\mathbb{R}} U \frac{dA^2}{dX} dX = n_0 (E_{\mathrm{cl}}^- - E_{\mathrm{cl}}^+). \tag{93}$$

In the r.h.s. of Eq. (93) we made use of relations (5) and (7).

It has been shown in Sec. III B that $E_{\mathrm{cl}}^- = 0$ and that under assumption (11) (small nonlinearity and arbitrary transmission or weak transmission and arbitrary nonlinearity) one has [see Eqs. (16) and (20)] $E_{\mathrm{cl}}^+ = 2\hbar^2\kappa^2/m(R/T)$, which yields

$$F_d = -\frac{2\hbar^2\kappa^2}{m} n_0 \frac{R}{T}. \tag{94}$$

In the regime $R \ll 1$, using Eq. (44) one recovers from Eq. (94) the perturbative result already obtained in Ref. [65]: $F_d = -2 n_0 m |\hat{U}(2\kappa)|^2/\hbar^2$ [66].

The physics embodied in Eq. (94) is rather simple and it is worth spending some time to discuss it. Consider an incident beam of particles with density n_{inc} and momentum $p = -\hbar\kappa$ moving from $+\infty$ toward an obstacle at rest. Part of the particles is transmitted (a fraction T) and the other part is reflected (a fraction R). The collisions are elastic and each of the reflected particles experiences an exchange of momentum $\delta p = 2\hbar\kappa$ with the obstacle. During a time δt there are N_{coll} collisions and by the law of action and reaction the obstacle experiences a force

$$F_d = -N_{\mathrm{coll}} \frac{\delta p}{\delta t} = -\frac{2\hbar^2\kappa^2}{m} n_{\mathrm{inc}} R. \tag{95}$$

In the r.h.s. of Eq. (95), one has written that $N_{\mathrm{coll}}/\delta t$ is the flux of particles colliding with the obstacle, i.e., $\frac{\hbar\kappa}{m} R n_{\mathrm{inc}}$. Equations (94) and (95) are identical because what we call n_0 is the downstream density of the beam (cf. Fig. 2), i.e., precisely $T n_{\mathrm{inc}}$. Depending on which quantity is held constant (n_0 as in the present paper, or n_{inc}), Eq. (94) or Eq. (95) is more appropriate (cf. the discussion of the fixed input and fixed output problem in Ref. [32]). This is somewhat reminiscent of the controversy on the correctness of the Landauer formula (see, e.g., the discussion in Ref. [67]).

On the basis of Eq. (94) one sees that the measure of $\dot{E}$ gives direct information on the transmission of the interacting beam through the disordered region, allowing one to reveal in which configuration is the system. For instance, in the localized regime the energy dissipation is high ($\propto 1/T$) and grows exponentially with the size L of the disordered region, whereas in the perturbative regime $\dot{E}$ is much lower and scales as L.

VII. CONCLUSION

In the present work we have presented an analysis of the transmission of a weakly interacting Bose gas incident on a disordered potential. We have shown on the basis of numerical and analytical results that there is a regime of Anderson localization in this system and proposed experimental signature of this phenomenon. In order to properly identify a "localized regime," we have studied the transmission coefficient and its probability distribution. The transmission coefficient T is well defined under assumption (11), which holds in the following regimes: (i) small nonlinearity and arbitrary transmission or (ii) weak transmission and arbitrary nonlinearity. In other cases there is no obvious way to define the transmission of the nonlinear beam because one cannot separate in the upstream region an incident flow from a reflected one. However, our analysis in terms of E_{cl} and λ (defined in Sec. III B) is always valid, even when condition (11) is not fulfilled. This just means that, out of regime (11), the connection (20) between λ and T is invalid. But, for instance, this

does not invalidate at all the analysis leading to the DMPK equation (66), and the experimental signature proposed in Sec. VI B also remains valid even when it is not possible to properly define T.

We note that the validity of the DMPK approach for noninteracting particles is a well-established fact in the theory of disordered systems. What is achieved in the present work is its extension to the case of interacting particles. Other studies of Anderson localization in the presence of interactions have concentrated on the long-time behavior of the time evolution of initial wave packets [68]. Although those results are still a matter of active debate in the community, the results of the present work produce strong evidence of the existence of Anderson localization for weakly interacting Bose particles (with effective repulsive interaction) propagating through disordered samples of finite size $L<L^*$.

Although the present study leads to the important conclusion that Anderson localization in the presence of interaction is possible, it is rather disappointing to remark that it can be clearly identified only when $V\gtrsim 20c$, i.e., in a regime where interactions do not play a major role (see the discussion of Sec. VI A and also Ref. [14]). In this respect, the more interesting effect of interactions is the existence of an upper threshold L^* for the length of the disordered region: for $L>L^*$ no stationary flow is possible. As shown in Sec. V C, L^* is directly connected to the probability distribution of the parameter λ and to the localization properties of the system. It would be very interesting to lead a systematic study of the transmission in the interaction-induced time-dependent regime ($L>L^*$) where the numerical results of Ref. [13] indicate a power-law decay of the time-averaged transmission, a signature generally considered as of loss of phase coherence, and onset of Ohmic behavior [69,70]. Work in this direction is in progress.

ACKNOWLEDGMENTS

It is a pleasure to thank B. Altshuler, A. Comtet, J.-L. Pichard, and C. Texier for inspiring discussions. This work was supported by ANR Grants No. 05-Nano-008-02, No. NT05-2-42103, and No. 08-BLAN-0165-01; by the IFRAF Institute; and by the Alexander von Humboldt Foundation. We gratefully acknowledge funding by the Excellence Initiative of the German Research foundation (DFG) through the Heidelberg Graduate School of Fundamental Physics (Grant No. GSC 129/1) and the Global Networks Mobility Measures the Frontier Innovation Fund of the University of Heidelberg. We furthermore acknowledge support through the DFG Forschergruppe 760 "Scattering systems with complex dynamics."

APPENDIX A: DISTRIBUTION OF REFLECTION COEFFICIENTS IN THE PERTURBATIVE CASE FOR A POTENTIAL OF TYPE (25)

We give here a demonstration of the perturbative results (46)–(48) in the special case of a Gaussian disordered potential U_g of type (25). A simple way to obtain this results starts by noticing that any Gaussian noise verifying $\langle \eta(x)\rangle=0$ and $\langle \eta(x)\,\eta(x')\rangle=\delta(x-x')$ [and here we are specifically interested in $\eta(x)$ that appears in Eq. (25)] can be written as (see, e.g., Ref. [71])

$$\eta(x)=\lim_{\nu\to\infty}\frac{1}{\sqrt{\nu}}\sum_{j=-\infty}^{+\infty}\epsilon_j\delta(x-X_j), \tag{A1}$$

where X_j's are random positions uniformly distributed on the real axis with density ν and mean spacing $1/\nu$, and $\epsilon_j=\pm 1$ is a random variable (with $\langle\epsilon_j\rangle=0$ and $\langle\epsilon_i\epsilon_j\rangle=\delta_{ij}$).

In order to calculate the probability distribution of the reflection coefficient R [whose value is given by Eq. (44)] one should first consider the distribution of

$$\hat{U}_g(2\kappa)=\int_{\mathbb{R}}dx\;U_g(x)e^{2i\kappa x}=\lim_{\nu\to\infty}\frac{\hbar^2\sqrt{\sigma}}{m}\frac{\hat{w}(2\kappa)}{\sqrt{\nu}}\sum_{j=0}^{\nu L}\epsilon_j e^{2i\kappa X_j}. \tag{A2}$$

The quantity $\hat{U}_g(2\kappa)$ as given by Eq. (A2) is formally equivalent to the position z of a particle performing a random walk in the complex plane after $N=\nu L$ iterations. The particle is initially at the origin and performs jumps of constant amplitude $s=(\hbar^2/m)|\hat{w}(2\kappa)|\sqrt{\sigma/\nu}$ with random direction. Denoting by $d^2P=p(z,N)dxdy$ the probability to find the particle in the domain $dxdy$ around z after N steps, if $N\gg 1$ [which is ensured by taking the limit $\nu\to\infty$ in Eq. (A2)], the central limit theorem yields

$$p(z,N)=\frac{1}{\pi N s^2}\exp\left(-\frac{|z|^2}{Ns^2}\right). \tag{A3}$$

It is then a simple exercise to get the distribution of $|z|^2$. One obtains

$$P(|z|^2,N)=\frac{1}{\langle|z|^2\rangle}\exp\left[-\frac{|z|^2}{\langle|z|^2\rangle}\right], \tag{A4}$$

where

$$\langle|z|^2\rangle=s^2N=\sigma(\hbar^2/m)^2|\hat{w}(2\kappa)|^2L. \tag{A5}$$

From relation (44), Eq. (A5) immediately yields the announced probability distribution (46) with

$$\langle R\rangle=\frac{m^2}{\hbar^4\kappa^2}\langle|z|^2\rangle=\frac{\sigma L}{\kappa^2}|\hat{w}(2\kappa)|^2. \tag{A6}$$

For a potential U_g of type (25), $|\hat{w}|^2=\hat{C}$ [see Eq. (30)] and Eq. (A6) demonstrates in this case the validity of Eqs. (47) and (48).

APPENDIX B: DERIVATION OF THE DMPK EQUATION (66)

In this appendix, we explain how to obtain the DMPK equation (66) starting from the discrete Langevin equation (62). Let us consider a generic situation where λ_n obeys a stochastic recursion relation of the type

$$\lambda_{n+1}-\lambda_n=F(\lambda_n,\zeta_n), \tag{B1}$$

with uncorrelated random variables ζ_n,

$$\langle \zeta_{n_1}\zeta_{n_2}\cdots\zeta_{n_N}\rangle = C_N\,\delta_{n_1 n_2}\cdots\delta_{n_1 n_N}. \tag{B2}$$

It is clear that, under assumption (63), Eq. (62) is of type (B1) with all the odd N averages in Eq. (B2) being zero and $C_2=1/2$ [cf. Eq. (64)].

Let $P(\lambda,n)d\lambda$ be the probability that λ_n lies in the interval λ, $\lambda+d\lambda$. One can express $P(\lambda,n)$ as

$$P(\lambda,n) = \langle \delta(\lambda_n-\lambda)\rangle = \left\langle \int_{\mathbb{R}} \frac{dk}{2\pi} e^{ik(\lambda_n-\lambda)} \right\rangle. \tag{B3}$$

This yields

$$\begin{aligned} &P(\lambda,n+1)-P(\lambda,n) \\ &= \left\langle \int_{\mathbb{R}} \frac{dk}{2\pi} e^{ik(\lambda_n-\lambda)}(e^{ikF(\lambda_n,\zeta_n)}-1) \right\rangle \\ &= \sum_{\ell=1}^{\infty} \frac{(-1)^\ell}{\ell!}\frac{\partial^\ell}{\partial\lambda^\ell}\left\langle F^\ell(\lambda_n,\zeta_n)\int_{\mathbb{R}}\frac{dk}{2\pi}e^{ik(\lambda_n-\lambda)}\right\rangle \\ &= \sum_{\ell=1}^{\infty} \frac{(-1)^\ell}{\ell!}\frac{\partial^\ell}{\partial\lambda^\ell}\langle F^\ell(\lambda,\zeta_n)\delta(\lambda_n-\lambda)\rangle. \end{aligned} \tag{B4}$$

Using the fact that λ_n depends on the variables $\zeta_1\zeta_2,\ldots,\zeta_{n-1}$ but not on ζ_n [as can be seen directly from Eq. (B1)] one can write the last of Eqs. (B4) as

$$P(\lambda,n+1)-P(\lambda,n) = \sum_{\ell=1}^{\infty}\frac{(-1)^\ell}{\ell!}\frac{\partial^\ell}{\partial\lambda^\ell}\{\langle F^\ell(\lambda,\zeta_n)\rangle P(\lambda,n)\}. \tag{B5}$$

In the case of Eq. (62) one has $F(\lambda,\zeta)=(1+2\lambda)/\kappa^2b^2+2(\lambda^2+\lambda)^{1/2}\zeta/\kappa b$ and the successive moments of F read

$$\langle F(\lambda,\zeta_n)\rangle = \frac{1+2\lambda}{\kappa^2b^2}, \tag{B6}$$

$$\langle F^2(\lambda,\zeta_n)\rangle = \frac{2(\lambda^2+\lambda)}{\kappa^2b^2}+O\left(\frac{1}{\kappa^4b^4}\right), \tag{B7}$$

with all the other moments being of order $1/(\kappa^3b^3)$ or more, i.e., negligible in regime (60). Equation (B5) thus reads

$$\begin{aligned} \kappa^2b^2[P(\lambda,n+1)-P(\lambda,n)] &= -\frac{\partial}{\partial\lambda}[(1+2\lambda)P]+\frac{\partial^2}{\partial\lambda^2}[(\lambda^2+\lambda)P] \\ &= \frac{\partial}{\partial\lambda}\left[\lambda(\lambda+1)\frac{\partial P}{\partial\lambda}\right]. \end{aligned} \tag{B8}$$

In the continuous limit, defining $t=n/(\kappa^2b^2)$, the l.h.s. of Eq. (B8) is simply the first derivative of P with respect to t, and Eq. (B8) reduces to Eq. (66) of the main text.

[1] P. W. Anderson, Phys. Rev. **109**, 1492 (1958).
[2] J. Billy *et al.*, Nature (London) **453**, 891 (2008).
[3] G. Roati *et al.*, Nature (London) **453**, 895 (2008).
[4] K. Huang and H. F. Meng, Phys. Rev. Lett. **69**, 644 (1992).
[5] S. Giorgini, L. Pitaevskii, and S. Stringari, Phys. Rev. B **49**, 12938 (1994).
[6] G. E. Astrakharchik, J. Boronat, J. Casulleras, and S. Giorgini, Phys. Rev. A **66**, 023603 (2002).
[7] D. Clément, P. Bouyer, A. Aspect, and L. Sanchez-Palencia, Phys. Rev. A **77**, 033631 (2008).
[8] Y. P. Chen, J. Hitchcock, D. Dries, M. Junker, C. Welford, and R. G. Hulet, Phys. Rev. A **77**, 033632 (2008).
[9] T. Giamarchi and H. J. Schulz, Phys. Rev. B **37**, 325 (1988).
[10] M. P. A. Fisher, P. B. Weichman, G. Grinstein, and D. S. Fisher, Phys. Rev. B **40**, 546 (1989).
[11] S. A. Gredeskul and Y. S. Kivshar, Phys. Rep. **216**, 1 (1992).
[12] N. Bilas and N. Pavloff, Phys. Rev. Lett. **95**, 130403 (2005).
[13] T. Paul, P. Leboeuf, N. Pavloff, K. Richter, and P. Schlagheck, Phys. Rev. A **72**, 063621 (2005).
[14] T. Paul, P. Schlagheck, P. Leboeuf, and N. Pavloff, Phys. Rev. Lett. **98**, 210602 (2007).
[15] C. Menotti and S. Stringari, Phys. Rev. A **66**, 043610 (2002).
[16] D. S. Petrov, G. V. Shlyapnikov, and J. T. M. Walraven, Phys. Rev. Lett. **85**, 3745 (2000).
[17] C. Raman, M. Kohl, R. Onofrio, D. S. Durfee, C. E. Kuklewicz, Z. Hadzibabic, and W. Ketterle, Phys. Rev. Lett. **83**, 2502 (1999).
[18] R. Onofrio, C. Raman, J. M. Vogels, J. R. Abo-Shaeer, A. P. Chikkatur, and W. Ketterle, Phys. Rev. Lett. **85**, 2228 (2000).
[19] P. Engels and C. Atherton, Phys. Rev. Lett. **99**, 160405 (2007).
[20] M. Olshanii, Phys. Rev. Lett. **81**, 938 (1998).
[21] A. D. Jackson, G. M. Kavoulakis, and C. J. Pethick, Phys. Rev. A **58**, 2417 (1998).
[22] P. Leboeuf and N. Pavloff, Phys. Rev. A **64**, 033602 (2001).
[23] L. P. Pitaevskii and S. Stringari, J. Low Temp. Phys. **85**, 377 (1991).
[24] M. Schwartz, Phys. Rev. B **15**, 1399 (1977).
[25] D. S. Petrov, Ph.D. thesis, University of Amsterdam, 2003; available online at http://www-old.amolf.nl/publications/theses/petrow
[26] A. V. Lopatin and V. M. Vinokur, Phys. Rev. Lett. **88**, 235503 (2002).
[27] G. E. Astrakharchik and L. P. Pitaevskii, Phys. Rev. A **70**, 013608 (2004).
[28] T. Ernst, T. Paul, and P. Schlagheck, e-print arXiv:0905.4750.
[29] V. Hakim, Phys. Rev. E **55**, 2835 (1997).
[30] H. Lamb, *Hydrodynamics* (Cambridge University Press, Cambridge, England, 1997).
[31] P. Leboeuf, N. Pavloff, and S. Sinha, Phys. Rev. A **68**, 063608 (2003).
[32] T. Paul, M. Hartung, K. Richter, and P. Schlagheck, Phys. Rev. A **76**, 063605 (2007).
[33] B. I. Ivlev and N. B. Kopnin, Adv. Phys. **33**, 47 (1984).
[34] J. S. Langer and V. Ambegaokar, Phys. Rev. **164**, 498 (1967).
[35] Note in particular that condition (11) is always fulfilled in the absence of interaction since in this case the speed of sound is $c\equiv 0$.

[36] B. I. Shklovskii and A. L. Efros, *Electronic Properties of Doped Semiconductors* (Springer-Verlag, Berlin, 1984).
[37] J. Fortágh and C. Zimmermann, Rev. Mod. Phys. **79**, 235 (2007).
[38] S. Kraft, A. Günther, H. Ott, D. Wharam, C. Zimmermann, and J. Fortágh, J. Phys. B **35**, L469 (2002).
[39] J. Estève, C. Aussibal, T. Schumm, C. Figl, D. Mailly, I. Bouchoule, C. I. Westbrook, and A. Aspect, Phys. Rev. A **70**, 043629 (2004); T. Schumm *et al.*, Eur. Phys. J. D **32**, 171 (2005).
[40] D.-W. Wang, M. D. Lukin, and E. Demler, Phys. Rev. Lett. **92**, 076802 (2004).
[41] J. W. Goodman, *Speckle Phenomena in Optics: Theory and Applications*, (Roberts and Company Publishers, Greenwood Village, 2007).
[42] D. Clément, A. F. Varón, J. A. Retter, L. Sanchez-Palencia, A. Aspect and P. Bouyer, New J. Phys. **8**, 165 (2006).
[43] L. Fallani, C. Fort, and M. Inguscio, Adv. At., Mol., Opt. Phys. **56**, 119 (2008).
[44] Equation (36) corresponds to a typical physical situation where the potential seen by the particles is proportional to the intensity of an electric field whose components are random Gaussian variables.
[45] In Ref. [14] this region has been improperly called "Ohmic."
[46] T. N. Antsygina, L. A. Pastur, and V. A. Slyusarev, Fiz. Nizk. Temp. **7**, 5 (1981); [Sov. J. Low Temp. Phys. **7**, 1 (1981)].
[47] I. M. Lifshits, S. A. Gredeskul, and L. A. Pastur, *Introduction to the Theory of Disordered Systems* (John Wiley, New York, 1988).
[48] O. N. Dorokhov, Pis'ma Zh. Eksp. Teor. Fiz. **36**, 259 (1982); [JETP Lett. **36**, 318 (1982)]; P. A. Mello, P. Pereyra, and N. Kumar, Ann. Phys. (N.Y.) **181**, 290 (1988).
[49] V. I. Mel'nikov, Fiz. Tverd. Tela (Leningrad) **23**, 782 (1981); [Sov. Phys. Solid State **23**, 444 (1981)].
[50] C. W. J. Beenakker, Rev. Mod. Phys. **69**, 731 (1997).
[51] P. A. Mello, J. Math. Phys. **27**, 2876 (1986).
[52] C. W. J. Beenakker and J. A. Melsen, Phys. Rev. B **50**, 2450 (1994).
[53] In order to complete the proof of this equivalence one has to show that the mean value $\langle \lambda \rangle = t = L/L_{\mathrm{loc}}(\kappa)$ obtained from Eq. (68) for a sample of length $X=L$ is identical to result (45). This amounts to show that for a potential of form (21) one has $\langle |\hat{U}_\delta(2\kappa)|^2 \rangle = (\hbar^2/m)^2 \sigma L$, which is easily obtained.
[54] A. A. Abrikosov, Solid State Commun. **37**, 997 (1981).
[55] B. A. Van Tiggelen, in *Diffusive Waves in Complex Media*, edited by J. P. Fouque (Kluwer Academic Publishers, Dordrecht, 1999), p. 1.
[56] Note that in Ref. [14] the theoretical determination of L^* was obtained using a criterion different from Eq. (80) resulting in a less precise estimate at high V/c.
[57] F. M. Izrailev and A. A. Krokhin, Phys. Rev. Lett. **82**, 4062 (1999).
[58] L. Sanchez-Palencia, D. Clement, P. Lugan, P. Bouyer, G. V. Shlyapnikov, and A. Aspect, Phys. Rev. Lett. **98**, 210401 (2007).
[59] L. Tessieri, J. Phys. A **35**, 9585 (2002).
[60] E. Gurevich and O. Kenneth, Phys. Rev. A **79**, 063617 (2009).
[61] P. Lugan, A. Aspect, L. Sanchez-Palencia, D. Delande, B. Gremaud, C. Muller, and C. Miniatura, Phys. Rev. A **80**, 023605 (2009).
[62] A. F. Ioffe and A. R. Regel, Prog. Semicond. **4**, 237 (1960).
[63] Note that the value $V^*/c=7.95$ does not depend on the type of correlation of the disordered potential considered since it is simply the value of V/c for which Eq. (81) admits the solution $t^*=1$.
[64] W. Guerin, J.-F. Riou, J. P. Gaebler, V. Josse, P. Bouyer, and A. Aspect, Phys. Rev. Lett. **97**, 200402 (2006).
[65] N. Pavloff, Phys. Rev. A **66**, 013610 (2002).
[66] Note that there is a factor of 2 difference between the present definition (14) of κ and the one used in Ref. [65].
[67] Y. Imry, *Introduction to Mesoscopic Physics* (Oxford University Press, Oxford, 1997).
[68] D. L. Shepelyansky, Phys. Rev. Lett. **70**, 1787 (1993); G. Kopidakis, S. Komineas, S. Flach, and S. Aubry, *ibid.* **100**, 084103 (2008); A. S. Pikovsky and D. L. Shepelyansky, *ibid.* **100**, 094101 (2008); S. Fishman, A. Iomin, and K. Mallick, Phys. Rev. E **78**, 066605 (2008).
[69] S. Datta, *Electronic Transport in Mesoscopic Systems* (Cambridge University Press, Cambridge, England, 1995).
[70] M. V. Berry and S. Klein, Eur. J. Phys. **18**, 222 (1997).
[71] C. Texier, Ph.D. thesis, Université Paris 6, 1999; available online at http://www.lptms.u-psud.fr/membres/texier/research.html